Interplate slip rate variation between closely spaced earthquakes in southern Mexico: The 2012 Ometepec and 2018 Pinotepa Nacional thrust events

L. A. Dominguez[1,5], T. Taira[2], V.M. Cruz-Atienza[3], A. Iglesias[3], C. Villafuerte[3,4], D. Legrand[3], X. Pérez-Campos[3], M. Raggi[1]

[1] Escuela Nacional de Estudios Superiores, Unidad Morelia. Universidad Nacional Autónoma de México, Morelia, México.

[2] Berkeley Seismological Laboratory, University of California, Berkeley, California, USA.

[3] Instituto de Geofísica, Universidad Nacional Autónoma de México, Mexico City, Mexico.

[4] Now at Laboratoire de Géologie, Département de Géosciences, École Normale Supérieure, PSL Université, Paris, France.

[5] Now at Instituto de Geofísica, Universidad Nacional Autónoma de México, Mexico City, Mexico.

Corresponding author: Luis A. Dominguez (ladominguez@igeofisica.unam.mx)

Key Points:

- The 2012 M_w 7.5 Ometepec-Pinotepa Nacional earthquake caused a long-term increase in the surrounding slip rates that lasted at least six years.
- Unlocking of a near the trench block favored the rupture of the 2018 M_w 7.2 Pinotepa Nacional earthquake.

- Coda wave interferometry analysis asserts that repeating earthquakes are caused by the same asperity.

Abstract

On 20 March 2012, a M_w 7.5 thrust earthquake started a series of large events up to magnitude M_w 8.2 (2017) that struck central Mexico during a period of nine years. Before this event, the Mexican subduction zone did not experience subduction earthquakes (M_w > 7.0) for at least 12 years. Most of the events during this highly active period (2012-) occurred in the plate interface, resulting in a significantly larger interplate slip rate in the states of Oaxaca and Guerrero. In this study, we explore how the aseismic slip transient caused by the 2012 M_w 7.5 earthquake affected the region and whether this earthquake had a causal relationship with a nearby similar magnitude event that occurred in 2018 (M_w 7.2). To this end, we identified and analyzed characteristic repeating earthquakes along the Mexican subduction zone for assessing the plate interface slip history and found a notably increase in the aseismic slip rate inferred from repeating earthquake activity following the 2012 mainshock, which suggests a long-standing slip perturbation in Oaxaca near the trench that continued until the 2018 M_w 7.2 Pinotepa Nacional earthquake.

Plain Language Summary

This study analyzes the large increase in seismicity and the changes in the plate interface motion that occurred between two major thrust earthquakes: The 2012 M_w 7.5 Ometepec earthquake and the 2018 M_w 7.2 Pinotepa Nacional earthquake. These two events, located in the state of Oaxaca in southern Mexico, were produced by two nearby asperities whose hypocenters were separated by only ~60 kilometers. To estimate the inter-seismic slip rates, we analyzed the occurrence of repeating events, a type of earthquake believed to be the result of asperities on the plate interface that rupture the same patch at relatively regular intervals. This kind of earthquake has extraordinarily similar waveforms that suggest a common origin in space and a similar rupture process. We explored the repeating earthquake activity and its characteristics to determine how the induced seismicity produced by the 2012 Ometepec earthquake influenced the rupture of the 2018 Pinotepa Nacional earthquake.

1. Introduction

An intense increase in seismic activity that may last from a few weeks or months through several decades often follows long quiescent seismic periods (Stein & Liu, 2009). While many earthquakes are clustered in both space and time (Barbot et al., 2012; Konca et al. 2008, Santoyo et al., 2005), others occur spontaneously with no clear triggering mechanisms (Corral et al., 2004; Kagan & Jackson, 1991; Kanamori 1981, Keillis-Borok et al., 1980; Wang et al., 2010; Wyss et al., 1988). In this regard, the Ometepec-Pinotepa Nacional region is a remarkable example of an area that experiences modulated periods of seismic activity. This segment, located along the central Pacific coast of Mexico at the border between the Oaxaca and Guerrero states, is well known for the occurrence of large earthquakes (> M7.0) that often take place as pairs of events interacting with each other during a relatively short period. The most striking example happened in 1982, when a magnitude M_s 7.0 earthquake was preceded by a M_s 6.9 earthquake within five hours (Astiz & Kanamori, 1984). Another duplet-type event occurred in 1928 when a magnitude M_S 7.6 was preceded by a M_S 7.4 two months before (Singh et al. 1981). A similar scenario occurred in 1962 to the West of the Ometepec-Pinotepa Nacional region, when a magnitude Ms 7.2 was followed by a M_s 6.9 only eight days apart (Nishenko & Singh, 1987, Ortiz et al., 2000). Furthermore, in

1995 and 1996, two earthquakes with magnitudes larger than 7.0 ruptured within a year (Anderson et al., 1995; Singh et al., 1997). Other magnitude M 7.0 events occurred as single earthquakes in 1937 (M_S 7.7), 1948 (M_S 7.0), 1950 (M_S 7.3), and 1968 (M_S 7.3) (see inset Figure 1). Recently, this area experienced two more earthquakes that ruptured a few years apart, the first one happened on 20 March 2012 (M_w 7.5) (UNAM seismology group, 2013) about 30 years after the 1982 doublet, and the second earthquake ruptured a nearby area, ~60km apart, on 16 February 2018 (M_w 7.2) (Li et al., 2020) (Figure 1). The aftershock sequence of the 2012 earthquake was particularly productive compared to other Mexican earthquakes located along the trench. This earthquake is characterized by a high Gutenberg-Richter *b* value (1.50 ± 0.10), and a low Omori p-value (0.37 ± 0.12). Furthermore, the modulation of the aftershocks rate by the Earth tides strongly suggest the presence of highly pressurized fluids at the plate interface in this Oaxaca region (Legrand et al., 2021). In this study, we evaluate the space-time evolution of the slip rate in this region between these two events the between 2012 and 2018 earthquakes and compared it with adjacent segments to understand the high seismicity rate in this area that has persisted for nearly a century of instrumental seismology.

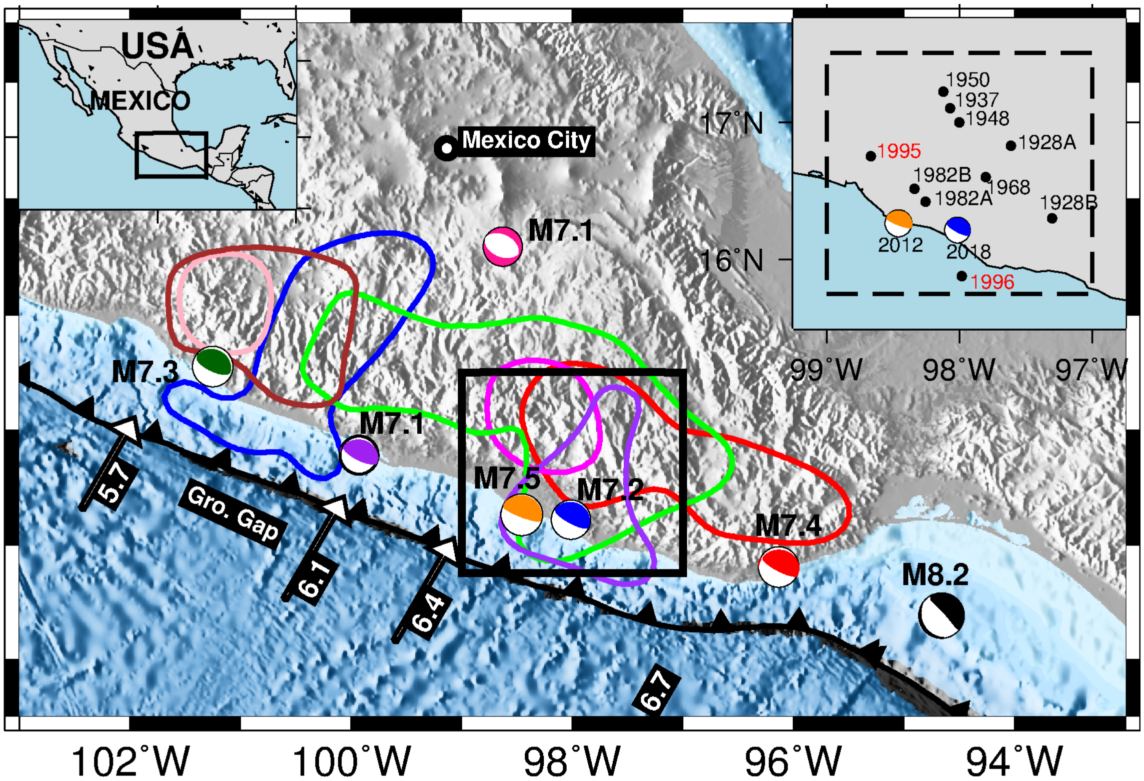

Figure 1. Major earthquakes in 2012-2020 in Mexico and significant seismicity in the Ometepec-Pinotepa Nacional region. Beach balls indicate the focal mechanisms of $M_w > 7$ earthquakes during the 2001-2021 period (Orange – 2012 Ometepec earthquake; green – 2014 Papanoa earthquake; blue – 2018 Pinotepa Nacional earthquake; black – 2017 Tehuantepec earthquake; pink – 2017 Puebla-Morelos earthquake; red – 2020 La Crucecita earthquake; purple – 2021 Acapulco earthquake). Colored contours show the rupture areas of the reported SSEs and the afterslip of the 2018 Pinotepa earthquake determined by Cruz-Atienza et al. 2021. Inset indicates known estimated hypocenters of large events ($M \geq 6.9$) since 1901 (Sawires et al. 2019). The black dashed rectangle indicates the region of interest.

Recent advances in seismic and geodetic monitoring, have provided new evidence about the possible mechanisms that cause such a high interplate slip rate compared to adjacent areas. Geodetic instrumentation shows that this area is constantly influenced by the occurrence of slow slip events (SSEs) downdip the Ometepec-Pinotepa Nacional segment every 1-2 years (~M6.0) which may have a strong influence on the occurrence of megathrust earthquakes in the region (Figure 1) (Cruz-Atienza et al., 2021; Graham et al., 2014). To the West, in the state of Guerrero, there is a region where no earthquakes with a magnitude larger than M>7.0 have occurred in more than a hundred years known as the Guerrero Gap (GG) (Singh et al., 1981; UNAM Seismology Group, 2015), where downdip SSEs take place every ~4 years. In addition, tectonic tremor is frequently observed as a by-product of SSEs (Cruz-Atienza et al., 2015, 2018; Husker et al., 2012, 2019; Kostoglodov et al., 2010; Payero et al., 2008; Plata-Martinez et al., 2021; Radiguet et al., 2012, 2016; Rivet et al., 2014; Vergnolle et al., 2010; Villafuerte & Cruz-Atienza, 2017). This variety of mechanisms has led to several hypotheses about the seismic budget distribution (Radiguet et al., 2012, Gualandi et al., 2017, Ramírez-Herrera et al., 2018) that suggest that a significant portion of the stress is released through aseismic slip in the seismic gap including its offshore segment (Plata-Martínez et al., 2021). If these hypotheses held true, the GG would not likely have yet the potential to nucleate large megathrust earthquakes by itself. Nonetheless, larger ruptures may be able to transit from either side as Plata-Martinez et al. (2021) hypothesized, which could lead to M>8.0 earthquake in Guerrero.

1.1 Tectonic Overview

The Mexican subduction zone is the result of the fragmentation of the Farallon plate that caused the oblique subduction of the oceanic Cocos and Rivera plates (Lonsdale 2005) beneath the continental North America plate. The resulting configuration produced a wide flat subducting slab that extends from the coast up to 250 km inland, flanked by segments with a steeper slope on both sides (Kim et al., 2013; Pardo & Suárez, 1995; Stubailo et al., 2012). The geometry of the slab has been explored using a wide range of techniques such as earthquake relocation (Pardo & Suarez, 1995), receiver functions (Melgar & Pérez-Campos 2011; Pérez-Campos et al., 2008), seismic ambient noise (Gaite et al., 2012; Spica et al., 2016), surface waves (Castellanos et al., 2018; Iglesias et al., 2010; Stubailo et al., 2012), body wave tomography (Husker et al. 2009) and seismic attenuation (Chen & Clayton, 2012). Flattening of the slab is likely due to dehydration and rollback that caused a shift in the volcanic arc which lies oblique with an angle of ~15° with respect to the trench, forming the Trans-Mexican volcanic belt with very diverse chemical signatures (Ferrari et al 2012, and references therein; Skinner & Clayton 2011). Another relevant feature for the regional tectonics consists of a continental left-lateral 650 km long fault system that extends parallel to the trench that accommodates a significant part of the oblique component of the subducting slab (Kazachkina et al., 2019, 2020). Both earthquake swarms and SSEs have been detected at the interface of this fault system in Oaxaca (Fasola et al., 2019).

1.2 Pore Pressure and Fluids in the Ometepec-Pinotepa Nacional Region

Considerable evidence suggests that the release of fluids controls the seismicity in this region. To the West, using magnetotelluric measurements in Guerrero, Husker et al. (2018) found a high conductivity zone on the upper layer of the subducting slab, which was associated with the presence of highly pressurized fluids as observed in different regions of the globe (Audet & Kim, 2016) and that may explain the migration pattern of tectonic tremor and SSEs cycles in that state and globally (Cruz-Atienza et al., 2018; Warren-Smith et al., 2019). In the Ometepec-Pinotepa segment, Plata-Martínez et al. (2019) examined the radiated energy of aftershock sequences of both the 2012 M_w 7.5 Ometepec-Pinotepa Nacional (hereafter 2012 Ometepec earthquake) and the

2018 M_w 7.2 Pinotepa Nacional earthquakes (hereafter 2018 Pinotepa earthquake). The ratio between the seismic energy to the seismic moment also suggests the presence of fluids along this zone. Elevated pore pressure can significantly reduce the effective normal stress allowing a higher seismicity rate compared to areas with lower fluid content. This was made clear by Legrand et al. (2021), who identified tidal-modulated aftershock seismicity following the 2012 M_w 7.5 Ometepec earthquake, and a high Gutenberg-Richter *b* value and low Omori *p* value, suggesting again the presence of over-pressurized fluids largely affecting the aftershock productivity. Fluids are often considered a major player that regulates the seismic activity that may result in large megathrust earthquakes (Audet & Schwartz 2013; Moreno et al., 2014) and quantitatively explain the cycle of slow earthquakes at the plate interface (Warren-Smith et al., 2019), including their associated rapid migrations (Cruz-Atienza et al., 2018).

2 Data

We extended the repeating earthquakes (REs, or repeaters) analysis, presented in Dominguez et al. (2016), by incorporating a longer time window ranging from 2001 through October 2021 (former results spanned from 2001 through 2014). Additionally, we carried out a complementary analysis of the rupture characteristics of the individual earthquakes to identify RE pairs. In total, we examined 440,655 vertical-component waveforms from 75,567 earthquakes (M>1.5) reported by the Servicio Sismológico Nacional (Pérez-Campos et al., 2018; SSN 2021). Figure S1 in the supplementary material shows the data availability and the number of records per event, as well as their magnitude distribution. Large gaps exist in the waveform data before 2006; therefore, caution must be taken in the interpretation of the results between 2001 and 2006. As of October 2021, all the stations have a sample rate of at least 100 Hz. Nonetheless, historical waveforms at some stations (i.e., CAIG - before 2008, MEIG - before, 2014, OXIG - before, 2007, PLIG - before, 2008, and PNIG - before 2007) are only available at 20 Hz, though. Therefore, we downsampled all records to 20 samples per second for our RE detections for this study. Notice that stations YOIG and PEIG were installed after the 2012 Ometepec earthquake. Thus, these stations will not be considered to evaluate temporal changes in RE activity before and after this earthquake.

3 Methods

3.1 Repeating Earthquakes

Repeating earthquakes are a type of event that consistently ruptures the same patch along the fault plane producing remarkably similar waveforms when examined at the same stations at different times (Poupinet et al., 1984; Vidale et al., 1994). Unlike most of the earthquakes which show complex and Poisson-type behavior, REs have relatively predictable recurrence times that scale with moment magnitude as ~$M^{1/6}$ (Catania & Seagall, 2019; Chen & Lapusta 2009; Nadeau & Johnson 1998;). REs are therefore considered the result of asperities that systematically accumulate and release stress with a similar moment magnitude in an otherwise aseismic slipping area. This process has been reported in a wide variety of tectonic environments such as oceanic fracture zones (Materna et al., 2018), transform faults (Nadeau & McEvilly, 1999, 2004; Uchida et al. 2019a; Vidale et al., 1994), volcanoes (Tepp 2018) and subduction zones (Chaves et al. 2020; Hughes et al. 2021; Mavrommatis et al., 2015; Uchida et al., 2015). Monitoring REs thus allows the estimation of the interplate aseismic slip as well as examining changes in the mechanical properties of the fault system. Nadeau & Johnson (1998) proposed an empirical relationship that links the interface slip around the seismogenic asperity, d, as a function of the RE coseismic moment, M_0, given by,

$$d = 10^a M_0^b, \tag{1}$$

where a and b are empirical constants. These authors suggested the following values a = -2.36 and b = 0.17 based on REs from Parkfield, California. Subsequent re-evaluations of these constants for the San Andreas fault suggested updated values of a = -1.09 ± 0.2 and b = 0.10 ± 0.02 (Nadeau & McEvilly, 2004); and a = -1.53 ± 0.37 and b = 0.10 ± 0.02 Koshmanesh et al., 2015.

We identified REs by comparing waveforms from pairs of nearby events (i.e., epicentral distances smaller than 50 km) reported in the SSN local catalog (SSN, 2021) with a 25 s time window from the onset of the *P* wave, which includes both *P*- and *S*- wave arrivals for events within 300km from the station. Data were demeaned, detrended and filtered using a Butterworth bandpass filter between 2-8 Hz. Then, we estimated the correlation coefficient and spectral coherency. We declared a pair of events as REs when both the correlation coefficient and the spectral coherence exceeded 0.95 for at least two stations. Sequences were initially formed by combining those pairs of events that shared a common reference earthquake into a single group. For example, suppose earthquakes A and C have a correlation coefficient and spectral coherency equal or higher than the given threshold (95%). In that case, we declare them as members of a RE sequence. Furthermore, suppose the waveform from a third event, earthquake B, meets the same similarity criterium compared to either earthquake A or C (not necessarily both). In that case, earthquake B is also a member so that all three events (A, B, and C) constitute a single sequence of REs. In the following sections, we detail our strategy to minimize false RE detections, which includes an additional constrain (unlike the study by Dominguez et al., 2016) where we estimated the relative distances between pairs of events using coda interferometry (Snieder & Vrijlandt, 2005) and inverted the results to make sure that the same asperity is indeed at the origin of the events instead of nearby asperities with a very similar earthquake to station path. The asperity size of each earthquake was determined independently through a stress drop estimate.

3.2 Stress drops calculation

To determine the size of the rupture patches and thus whether a sequence of repeaters was produced by the same asperity or by a nearby asperity, we first computed the stress drop of each seismic event based on Brune's model (Brune, 1970). Our procedure is similar to that proposed by Ordaz & Singh (1992), although we solved for the stress drop assuming the attenuation laws presented in García et al., (2009). The observed spectrum at the station *i* for the *j* event may be expressed as

$$A_{ij}(f, R_{ij}) = C \cdot S_j(f) \cdot G(R_{ij}) \cdot e^{-\pi f \cdot R_{ij} \beta Q(f)}, \quad (2)$$

where f is the frequency, R_{ij} is the hypocentral distance, $G(R_{ij})$ is the geometrical spreading, $Q(f)$ is the attenuation, and

$$C = \frac{R_{\theta\phi} F}{4\pi\rho v^3} \quad (3)$$

In this equation, $R_{\theta\phi}$ = 0.55 represents the average radiation pattern (Boore & Boatwright, 1984), F = 2. 0 accounts for the free surface amplification, v is the *P*-wave velocity ($6230 m/s$), and the density $\rho = 2.7 g/cm^3$ (Garcia et al., 2004). We used a path-dependent attenuation function and distance-dependent geometrical spreading as shown in García et al. (2009) for the Mexican subduction zone where $Q_S(f) = 175 f^{0.52}$ for coastal paths and $Q_S(f) = 211 f^{0.46}$ otherwise. To estimate the equivalent $Q_P(f)$ attenuation, we considered that $Q_p^{-1} = (4/9) Q_S^{-1}$ for a Poisson solid (Shearer 2019), assuming the same frequency dependance. Thus, we obtained $Q_P(f) = 394 f^{0.52}$ for coastal paths and $Q_P(f) = 475 f^{0.46}$ otherwise. The geometrical spreading is defined as,

$$G(R) = \begin{cases} 1/r, & for\ r < 50km \\ 1/\sqrt{50r}, & for\ r \geq 50km \end{cases}, \quad (4)$$

for coastal paths, and

$$G(R) = \begin{cases} 1/r, & for\ r < 50km. \\ 1/50, & for\ 50 \leq r \leq 150km \\ \sqrt{3}/\sqrt{50r}, & for\ r \geq 150km \end{cases} \quad (5)$$

for trajectories towards the continent. For the instrument response, we applied a prefilter with the following corner frequencies f_c = 0.005, 0.0125, 30, 40 Hz. After correcting path effects, we took a P- wave time window of 1.28s (128 samples at 100 sampling rate) and applied a 5% taper to the signal. Brune's model allows estimating the source dimensions from the power spectra of either the P- wave or the S- wave at the source, which can be approximated as,

$$S(f) = \frac{\Omega_0(2\pi f)^m}{1+(f/f_c)^2}, \quad (6)$$

where $S(f)$ is the spectrum of the seismic recording after removing the geometrical spreading, attenuation, and the instrument response. m is a factor that is applied in the frequency domain depending on whether the spectrum is on displacement ($m = 0$), velocity ($m = 1$) or acceleration ($m = 2$), f_c is the corner frequency and Ω_0 is the flat level at low frequencies in the displacement spectrum. We used a multitaper spectrum library to estimate the spectrum as shown by Prieto et al., (2009) and fit the resulting spectrum for all three possible combinations of spectra (displacement, velocity and acceleration) for the vertical component. Then, we estimated the coefficient of determination, R^2, and thus evaluated the goodness of the fitting. R^2 was computed as,

$$R^2 = \left(1 - \frac{U_{residual}}{U_{total}}\right) \times 100, \quad (7)$$

where $U_{residual} = \sum(u_{obs} - u_{Brune})^2$ is the sum square of the residuals. $U_{Total} = \sum(u_{obs} - \bar{u})^2$ is the total sum of squares, and $\bar{u}$ indicates the mean value of the observed data. Finally, we estimate the stress drop, $\Delta\sigma$, as a function of the estimated seismic moment M_0 and the corner frequency f_c,

$$\Delta\sigma = \frac{7}{16}\left(\frac{f_c}{\kappa\beta}\right)^3 M_0. \quad (8)$$

In this case, κ = 0.32 (Madariaga 1976) and β is the *S*-wave velocity (3.9 km/s) in the crust (Dziewonski & Anderson, 1981). To evaluate the stress drop for each cluster, we took the average values of the best fitting spectra with signal-to-noise ratio, $SNR \geq 5$, and $R^2 \geq 80\%$. Examples of the fittings are shown in the Figures S2, and a summary of the results is provided in the supplementary material Dataset S1.

3.3 Inter event distance and relative positions

When two closely spaced asperities produce repeating earthquakes, the recorded waveforms exhibit a large correlation and coherence value. In this case, they can be produced either by a partial rupture of a larger asperity or by nearby independent asperities located a few meters apart (Uchida, 2019). We assumed that each rupture could be modeled as an instantaneous penny-shape circular crack whose radius is estimated from their moment magnitude and stress drop (Eshelby 1957),

$$R = \left(\frac{7}{16}\frac{M_0}{\Delta\sigma}\right)^{1/3} \quad (9)$$

where M_0 is the moment magnitude in Nm, and $\Delta\sigma$ is the stress drop in MPa. The relative distance between pairs of events was computed employing coda wave interferometry (Snieder & Vrijlandt, 2005). Figure 2 illustrates an example of this process. Figure 2a shows the waveforms of sequence 0406 that containing eight REs. First, we aligned all the waveforms to the P- wave using a cross-correlation of the entire waveform in a 51 s window. Analysis of the correlation coefficient starts in the coda, which we assumed starts at twice the S-P arrival time. Then, we vary the window length and measure the distance in a 5 s window at three times the S-P arrival time from the onset of the *P* wave. Figure 2b shows the variations of the correlation coefficient as a function of the window length, and Figure 2c shows the corresponding interevent distance, as described by Snieder & Vrijlandt (2005), for all possible pairs.

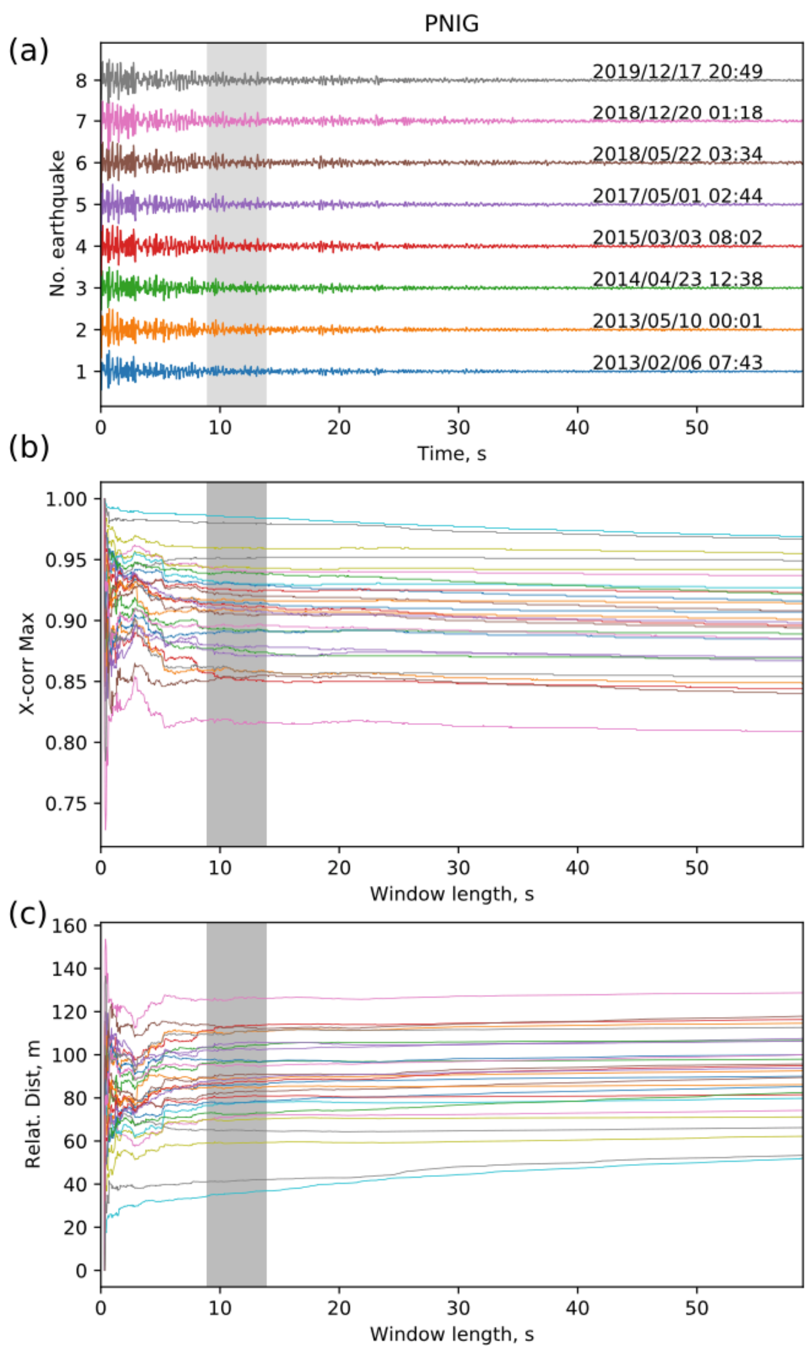

Figure 2. Coda wave interferometry results for sequence 0406. This RE sequence consists of eight members with a mean duration magnitude of M_d=3.9. (a) Individual waveforms, the gray shaded area indicates the time window where the relative distance between events is calculated. (b)

Maximum cross-correlation and (c) Relative distance between each pair of events. Time t = 0, corresponds to twice S-P time measured from the onset of the P wave.

Once we obtained a set of inter-event distances for each RE sequence, we determined a plausible configuration of the hypocenter at the plane interface. To invert the relative inter-event positions estimated by means of coda wave interferometry, we used a differential evolution algorithm approach (Storn & Price, 1997). This optimization method maintains a population of individuals (i.e. candidate solutions) that gradually minimize an objective function. In our cause, individuals are the hypocentral locations of each event along the same fault plane so that for every set of points is lying in the plane; the method finds the pairwise distance matrix D_P, where $D_P[i,j] = d(P_i, P_j)$. Among all such pairs, P, the optimal event locations are those minimizing the objective function $d(D, D_P)$. Each generation is constructed from the previous one. In this sense, differential evolution can be thought of as a primitive genetic algorithm. This method, in a nutshell, maintains a population of individuals that gradually improve. Therefore, each generation is constructed from the previous generation. To perform differential evolution, we start with a population of random individuals. Then, we successively repeat the following procedure: In each generation, for each individual P in the current population, we choose three other individuals A, B, and C; and use them to construct a new candidate individual, which we will call, $\tilde{P}$. This candidate $\tilde{P}$ is compared against P, and replaced it in the next generation if its associated cost function is lower. This process continues until no more improvements are to be found; see Storn & Price (1997) for further details.

Figure 3 illustrates the process described above to examine sequence 0203. The estimated average stress drop for this sequence inferred from Brune's model fitting is $\Delta\sigma = 0.12 \pm 0.07$ MPa. The radius of the asperity is then computed using Eq. 9. In this case, we assigned the same radius to all members based on their estimated stress drop and M_0. Figure 3a shows a possible plane solution of relative locations and size of the asperity based on the inversion of their relative distances estimated using coda wave interferometry as explained previously. Notice that any rotation of the reference system will also be a solution to that specific set of relative distances. Figure 3b shows the dendrogram which indicates whether the members within the same sequences can be associated with a single asperity or not. In this specific example, the diagram suggests that a stress drop of at least $\Delta\sigma = 30$ MPa is required to obtain a separation distance short enough ($r_{critical} = 187$ m) to consider the earthquake 09901800.02 as an independent asperity. Therefore, in this case, we conclude that all earthquakes within the sequence belong to the same asperity given the estimated stress drop and their relative interevent distances.

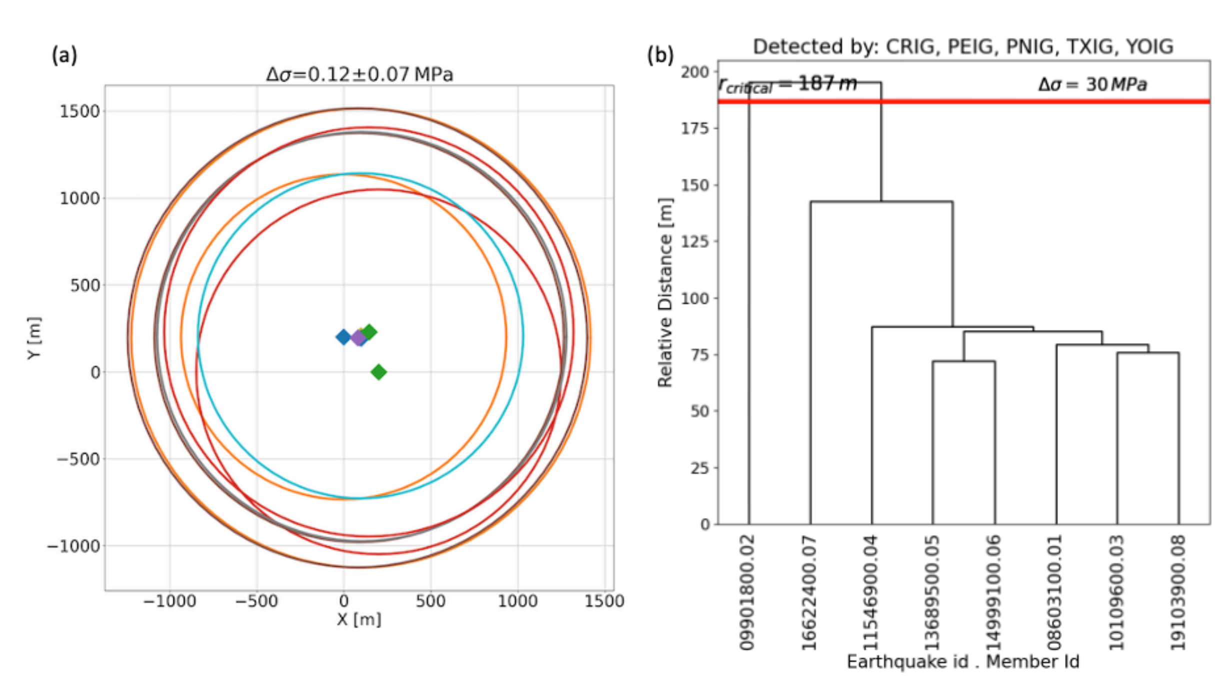

Figure 3. Relative locations and dendrogram of the sequence 0203. a) Estimated relative locations and estimated rupture area for all events within the sequence. b) Dendrogram, the *x*-axis indicates the earthquake id and the consecutive member id within the sequence, the *y* axis indicates the relative distance.

3.4 Completeness of the RE Catalog

Since our RE detections detach from waveform templates of earthquakes reported by the SSN, our catalog's spatial completeness (i.e., the geographic extent with the same cut-off magnitude) of our catalog is tied to the detectability of the SSN instrumental network. Once stations YOIG and PEIG were installed in 2012, a completeness analysis of the station network (Figure S3) indicates that the current cutoff magnitude (Mc) is about 3.3 for the whole extent of our study area. However, to avoid apparent changes in the seismicity rate due to detectability artifacts in our long-term RE time series ranging between 2002 and 2020, we determined a sufficient minimum completeness value $M_c = 3.8$ which implies that most of the events above this magnitude have similar locations and focal mechanisms to the template earthquakes in our catalog within the geographic extent. In the following section, we will not consider any detection below this threshold to assure that our interpretations are not influenced by improvements in the network. Nonetheless, complementary figures containing all detections are provided in the Supplementary Material.

4 Results and discussion

We found a set of 476 RE sequences that contain between 2 and 25 members with magnitudes ranging from 3.0 to 4.5 (see Supplementary Material, Dataset S2). The locations of the sequences are color-coded according to their magnitude in Figure 4. As discussed above, on this map, we only include events that meet a strict completeness criterion of the earthquake catalog across the study region during the whole analyzed period (for a map including all detected RE see Figure S4). Notice that the GG and Puerto Escondido (i.e., close to PEIG station) segment stands out as areas with a lower concentration of REs compared to adjacent areas likely perturbed by the large subduction earthquakes. In comparison, the area of interest (Ometepec-Pinotepa Nacional region) exhibits a noticeable larger RE activity, as well as the offshore region of the 2014 Papanoa earthquake.

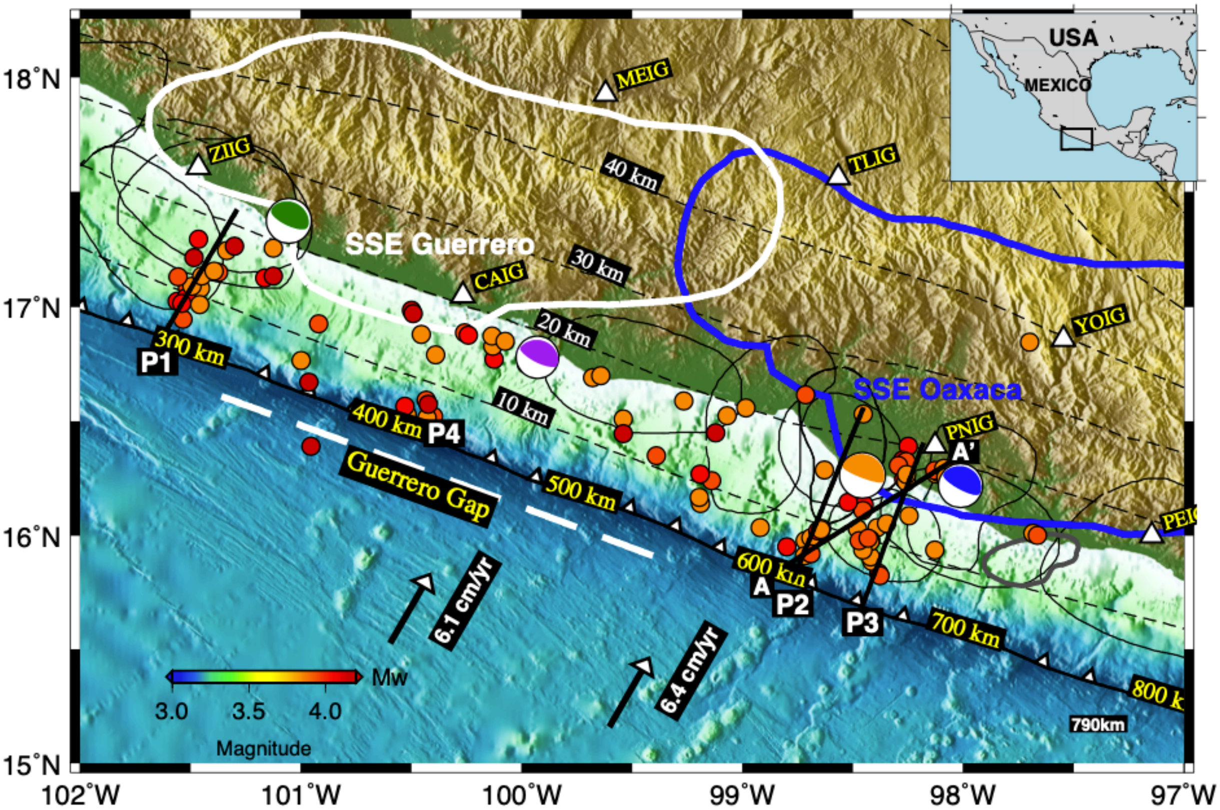

Figure 4. Detected RE sequences along the Guerrero and Oaxaca megathrust above $M_c \geq 3.8$. Triangles indicate the location of the permanent seismic stations used in this study. The white dashed line shows the extension of the Guerrero Gap. Thick black lines indicate the location of the four profiles examined in this study. Focal mechanisms correspond to the recent $M_w > 7.0$ earthquakes: 2014 Papanoa earthquake (green), 2012 Ometepec earthquake (orange), 2018 Pinotepa earthquake (blue) and 2021 Acapulco earthquake (purple). RE clusters are indicated by circles color coded by mean magnitude. Black dashed lines show the slab iso-depth as shown by Cruz-Atienza et al., (2021). Black closed contours represent rupture areas of large earthquakes

(Kostoglodov & Pacheco, 1999). Thick contours approximate areas of SSE ruptures areas in Guerrero (white) and Oaxaca (blue) (Graham et al., 2014).

In Figure, 5 we compare the changes in RE activity and interplate slip rates across both the Ometepec-Pinotepa Nacional and GG regions. Notice the drastic change in seismicity and, consequently, the number of REs following the 2012 Ometepec earthquake in the former case. In Figure 5a, we show the timing of significant nearby earthquakes ($M_w \geq 6.0$) (blue and red dots for Oaxaca and Guerrero, respectively), the approximate duration of SSEs in Guerrero (red shaded areas) and Oaxaca (blue shaded areas), and the number of REs reported as a function of time in 2-month bins. We included in this plot the 2017 M_w 7.1 Puebla earthquake (Melgar et al., 2018a; Singh et al., 2018), given their magnitude and societal impact. However, this event ruptured ~250 km from the trench in the bending section of the slab and no static or dynamic transfer of stress has been found (Cruz-Atienza et al., 2021; Segou & Parsons, 2018). Cumulative RE counts show that the Ometepec-Pinotepa Nacional segment almost doubled the activity observed in the GG during the same period (panel b).

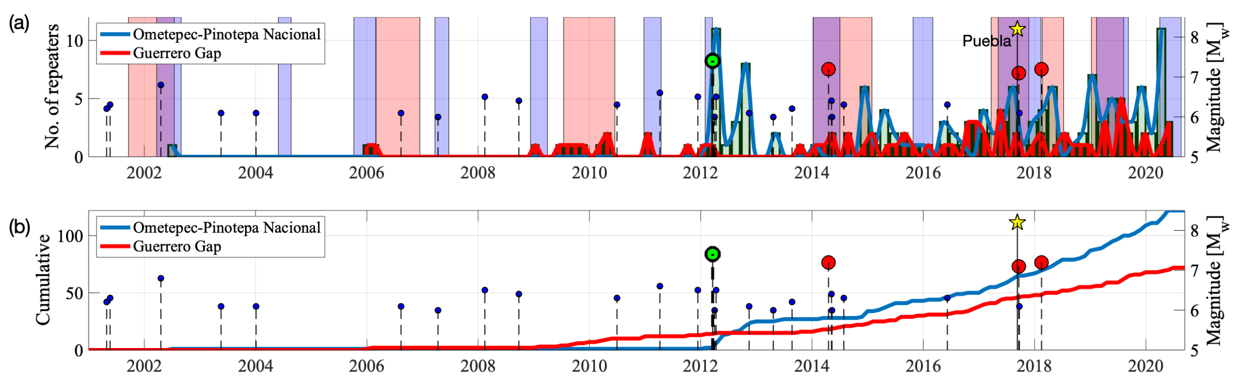

Figure 5. Major earthquakes and cumulative number of REs in the Ometepec-Pinotepa Nacional region (black square in Fig. 1). (a) Number of REs detected in the region in two-month bins (blue line). Red shaded areas show SSEs in Guerrero, while blue areas show the time intervals of the

SSEs in Oaxaca. (b) Cumulative number of REs in the Ometepec-Pinotepa Nacional region (blue line) and the Guerrero Gap (red). Blue steams denote earthquakes with magnitudes larger than $M_w > 6.0$, red stems, earthquakes with $M_w > 7.0$ and the green stem indicates the 2012 Ometepec earthquake. The yellow star marks de M_w 8.2 Tehuantepec earthquake.

To compare the RE recurrence time interval with studies worldwide, we evaluated the recurrence times for the RE catalog as a function of the seismic moment, M_0. Figure 6 shows the results color-coded by their position along the trench, as indicated in the inset. REs along the Guerrero Gap (red-orange colors – diamond markers) have recurrence times ranging between 1 and 10 years, which are generally consistent with the Nadeau & Johnson (1998) relationship (black dashed line) after correcting for the local slip rate (i.e., the plate convergence rate) as shown in Chen et al. (2007). In contrast, the Ometepec-Pinotepa Nacional region (yellow-green colors) shows much shorter recurrence times likely due to the co- and post-seismic perturbations induced by both the 2012 Ometepec and 2018 Pinotepa earthquakes. Another way to see this is shown in Figure 7, where the large differences in the recurrence times between the Ometepec-Pinotepa Nacional and adjacent segments are clear, dropping below the 1-month threshold in the former case. On the other hand, the post-seismic relaxation produced by the 2014 Papanoa earthquake in Guerrero had a small effect on the recurrence times compared with nearby sequences, such as the GG, where recurrence times of most of the REs range between 1 and 10. A similar plot including all the stations available after 2012 including all detected events is shown in Figure S5.

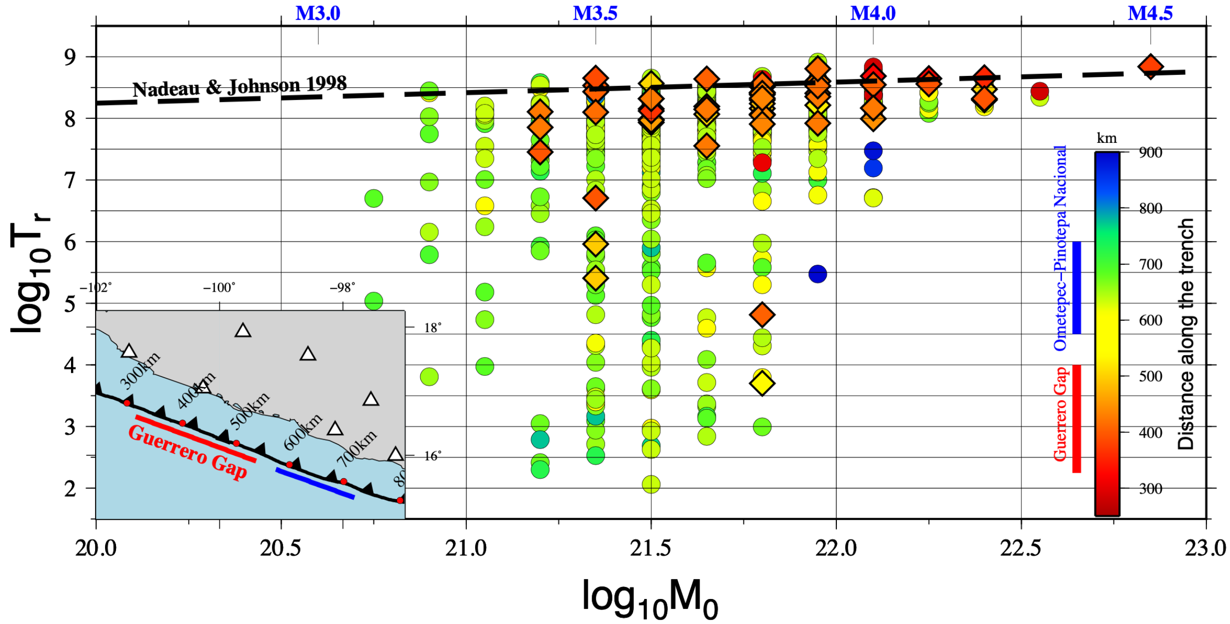

Figure 6. Comparison between the recurrence times along the Guerrero Gap and the Ometepec-Pinotepa Nacional region. Colors indicate the distance along the trench as indicated in the inset, diamond-type markers indicate the recurrence times of REs along the GG. The dotted line indicates

the expected recurrence times from the empirical relationship proposed by Nadeau & Johnson (1998).

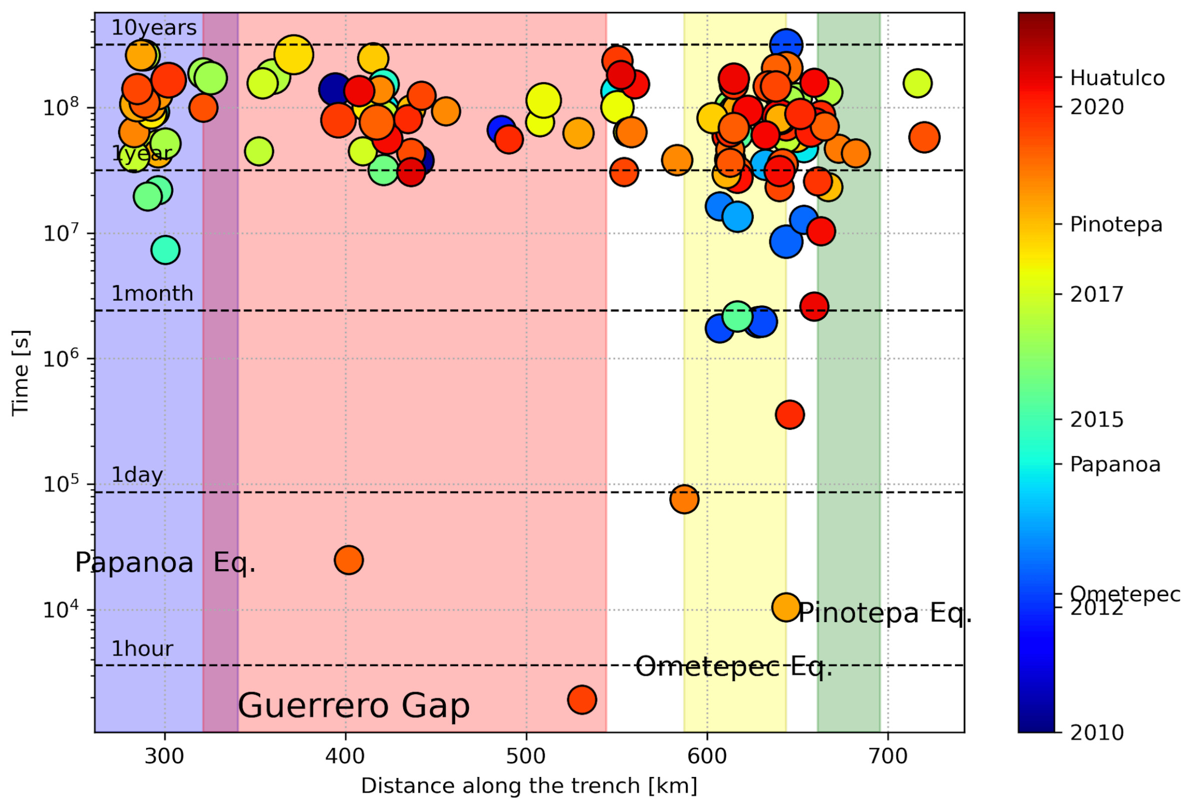

Figure 7. Recurrence times of reported RE pairs color-coded by the recurrence time. The size of the circles is proportional to the average magnitude of the events. Shaded areas show the projected rupture areas of the 2014 Papanoa earthquake (blue), the Guerrero Gap (red), the 2012 Ometepec earthquake (yellow) and the 2018 Pinotepa earthquake (green). Only REs above the $M_C \geq 3.8$, excluding data from stations PEIG and YOIG are shown in this plot.

To investigate possible changes in the slip rates along the adjacent areas of the rupture zones, we grouped the REs along four profiles as indicated in the map shown in Figure 4 (in each group we include all epicenters within 10 kilometers of the lines). Profile P1 corresponds to a line perpendicular to the trench that aims towards the rupture area of the 2014 Papanoa earthquake west of the GG. Note that the 2014 Papanoa rupture took place during the 2014 Guerrero SSE, which likely acted as a triggering mechanism of the earthquake (Radiguet et al., 2016; UNAM Seismology Group, 2015). Figure 8 shows the evolution of the RE activity along this profile. RE detections start six years before the earthquake and updip, between 15 and 30 km from the trench, indicating possible slip acceleration in the shallow part of the plate interface. After the mainshock, new sequences developed downdip near the hypocenter, certainly associated with the postseismic relaxation for two years following the event. Southeast of the study region, profiles P2 and P3 (figures 9 and 10, respectively) are parallel lines that extend approximately towards the rupture areas of the 2012 Ometepec and 2018 Pinotepa earthquakes. These profiles show a more intense aftershock activity that concentrates in the two different depth ranges, downdip around the 20 km depth interface isoline and around the 10 km depth isoline. The 2012 Ometepec and 2018 Pinotepa earthquakes nucleated at depths between 10 and 20 km, where the seismicity is significantly lower and where almost no repeaters are observed both before and after the events. This suggests the existence of either a relatively locked or freely slipping (stable) trench-parallel segment with 20 to 30 km in length along dip. Unlike profile P3, profile P2 shows a delayed activation of REs that first happened in the shallow, near the trench segment (about six months after the 2012 Ometepec earthquake) and then in the deeper segment about three years later. In Profile P3, RE activity began immediately after the mainshock in both segments with more intensity in the shallow one.

The most outstanding feature of the RE activity is the absence of repeaters for more than a decade before the 2012 earthquake, especially in the Ometepec region (figures 9 and 10). After this event, seismicity (and REs) largely increased, as expected from the afterslip of the 2012 and 2018 earthquakes (UNAM Seismology Group, 2013, 2015). The activation of REs (most of them offshore) from the occurrence of the 2012 event suggests two possibilities: (1) that the shallow plate-interface region mechanically transitioned from a predominantly locked to a weaker slipping regime when the earthquake happened; or (2) that the downdip segment unlocked after the event and pulled down (over-stressed) the shallow block increasing the strain release rate updip. In both cases, the shallow offshore segment seems to have evolved from a quasi-static, creeping regime to an aseismic stress-releasing state (Wang & Dixon, 2004). Although the first hypothesis is plausible due to dynamic weakening of the fault gauge materials due to large seismic waves (Cruz-Atienza et al., 2021; Johnson et al., 2012), we favored the second hypothesis since the magnitude of both Oaxaca earthquakes is relatively small (and consequently their waves amplitude and duration). However, sustained seismic and RE activity until 2021 could certainly be explained by the regional plate interface softening produced by seismic waves of the great M_w 8.2 (2017) Tehuantepec earthquake (Melgar et al., 2018b; Meng et al., 2019; Suárez et al., 2019), which strongly disturbed the SSE cycles in Guerrero and Oaxaca (Cruz-Atienza et al., 2021).

Several empirical relationships have been proposed to estimate the fault slip at the interface based on the RE magnitude. Comparison between these relationships (figures 8 through 10, panel a) shows very large differences that range from near plate convergence speed (Nadeau & Johnson, 1998) to near full coupled (Koshmanesh et al., 2015). Little can be said from this comparison. However, since the stress-releasing afterslip of both earthquakes spread partly across the RE locations, especially those below 10 km depth (Cruz-Atienza et al., 2021; Graham et al., 2014), the relationship proposed by Koshmanesh et al. (2015) is clearly inappropriate for Oaxaca as it does not predict slip rates larger than the plate convergence velocity after the events. Precise parameter calibration in space and time requires further investigation to determine the best set of parameters ($a,$ and b, see Eq. 1) that better describe the slip along the interface for the Mexican subduction zone.

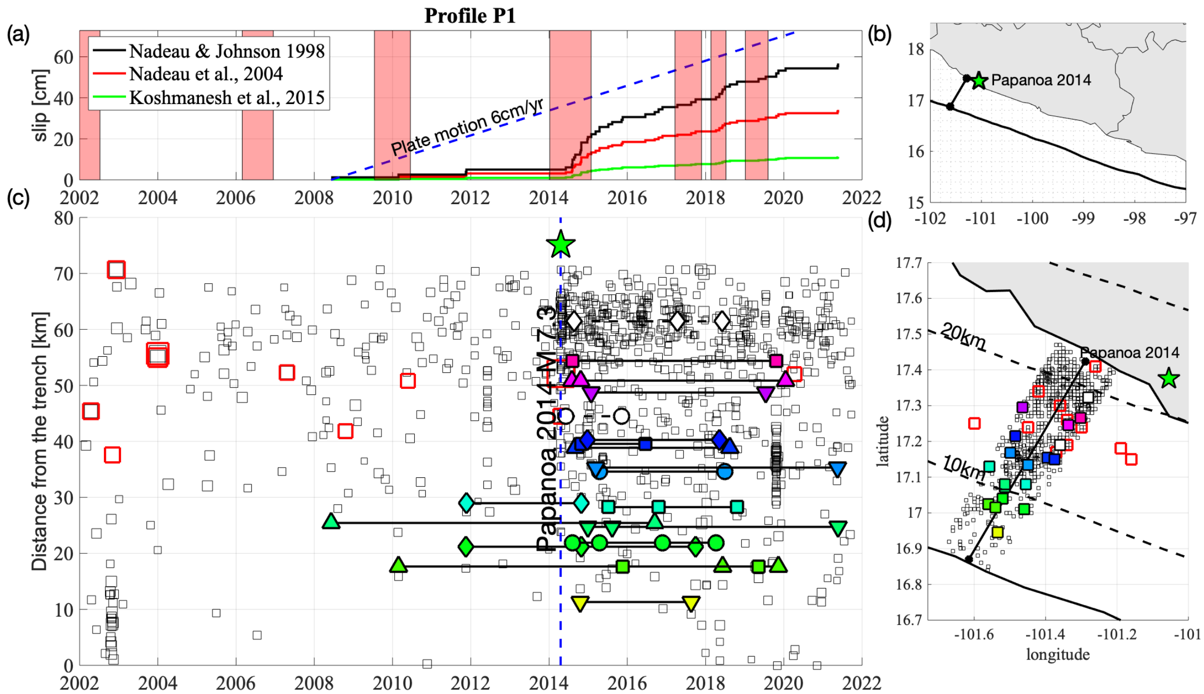

Figure 8. Seismicity and RE activity along a profile P1, near the 2014 Papanoa earthquake (see Fig. 4). (a) Estimated slip rates based on three empirical relationships (see main text), red shaded areas show the time windows for the SSE in Guerrero. (b) Location map. (c) Temporal evolution of the seismicity before and after the 2014 Papanoa earthquake. Black squares indicate the reported seismicity along a 10 km strip at each profile side. Colored symbols indicate the occurrence of REs (white markers show REs below $M_d < 3.8$); red squares indicate M≥5.0. (d) Map view of the profile. Background seismicity is shown as empty squares; REs within in a 10 km distance from the profile, M≥5.0 within a 20 km distance from the profile are denoted by red open squares and the location of the 2014 Papanoa earthquake by the green star.

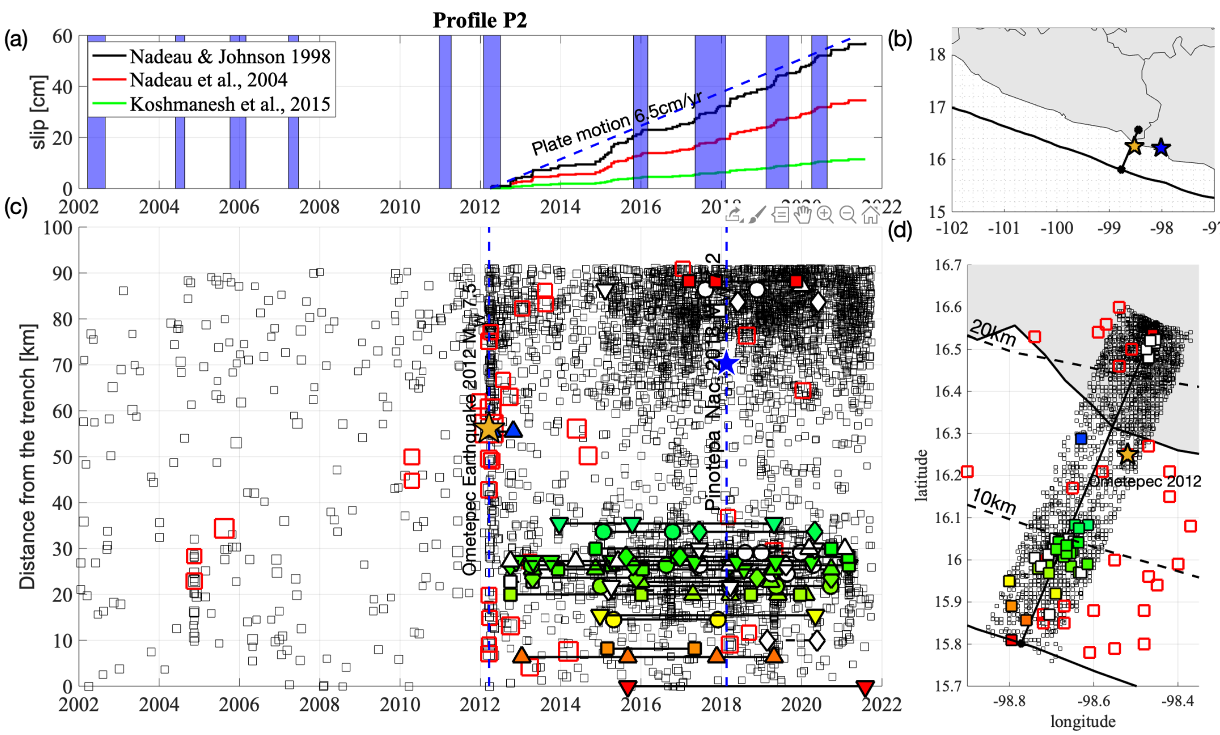

Figure 9. Seismicity and RE activity along a profile P2 near the 2012 Ometepec and 2018 Pinotepa earthquakes (see Fig. 4). (a) Estimated slip rates based on three empirical relationships (see main text), blue shaded areas show the time widows for the SSE in Oaxaca. (b) Location map. (c) Temporal evolution of the seismicity, black squares indicate the reported seismicity along a 10 km strip at each side profile side. Colored symbols indicate the occurrence of REs (white markers show REs below the $M_d < 3.8$). (d) Map view of the profile. The seismicity is shown as empty black squares; REs as symbols color-coded by distance to trench; the stars indicate the location of the 2012 Ometepec (blue) and 2018 Pinotepa (red) earthquakes.

Figure 11 shows the temporal distribution of the RE clusters projected along the trench as indicated in the map of Figure 4. Although we carefully determined the completeness cutoff magnitude for the whole region considering only available stations before 2012, the deficit of REs between 2001 through 2006 can be partially attributed to a sparser network and gaps in the data, as shown in Figures S1 and S2. However, the total absence of REs in the Oaxaca segment between 2006 and the 2012 Ometepec earthquake suggests a strong interface coupling in that period. By contrast, the opposite situation seems to dominate after this event, where large and sustained RE activity is found, i.e., a large and sustained increase of the interplate slip rate. This conjecture is independently supported by the long-term GPS data in Pinotepa Nacional (i.e., PNIG station) (Figure 12). Until the 2012 Ometepec earthquake, the station followed a steady-state northward motion as expected at this site by the regional plate convergence. However, after the rupture of the 2012 Ometepec earthquake, a large postseismic rebound was observed that lasted until 2016. During the four years of postseismic relaxation, the site steadily moved seawards (southward), indicating interplate slip rates larger than the plate convergence velocity. After the relaxation, the displacement partially recovered its interseismic regime to the north until the great 2017 M_w8.2 Tehuantepec earthquake perturbed the entire region, most likely leading the 2018 M_w 7.2 Pinotepa earthquake (Cruz-Atienza et al., 2021). In other words, during 2016 and until the Tehuantepec rupture on 8 September 2017, the upper plate at PNIG moved northward with speed smaller than the long-term expected velocity, which suggests a large creeping rate at the interface. These independent observations are consistent with the sustained increase of REs activity in the region between the Ometepec (2012) and Pinotepa (2018) earthquakes (Figures 9 and 10).

Conversely, along the GG, REs show a more sustained behavior, probably affected by the occurrence of SSEs in Guerrero, as suggested in Figure 5. Before the 2006 SSE, repeaters preceded the onset of the event while during the 2009-2010 SSE, RE activity increased during this event as well as during the 2014 SSE. The 2014 Papanoa earthquake gave rise to both activation of new RE clusters and reactivation of previously identified clusters mostly towards the west side of the rupture farther from the border of the GG, while inside the GG, a larger population of REs emerged after the 2014 SSE. A complementary and equivalent figure showing all the detected REs including those below our estimated time-independent magnitude of completeness (i.e., Mc=3.8) is provided in the Supplementary Material, Figure S6.

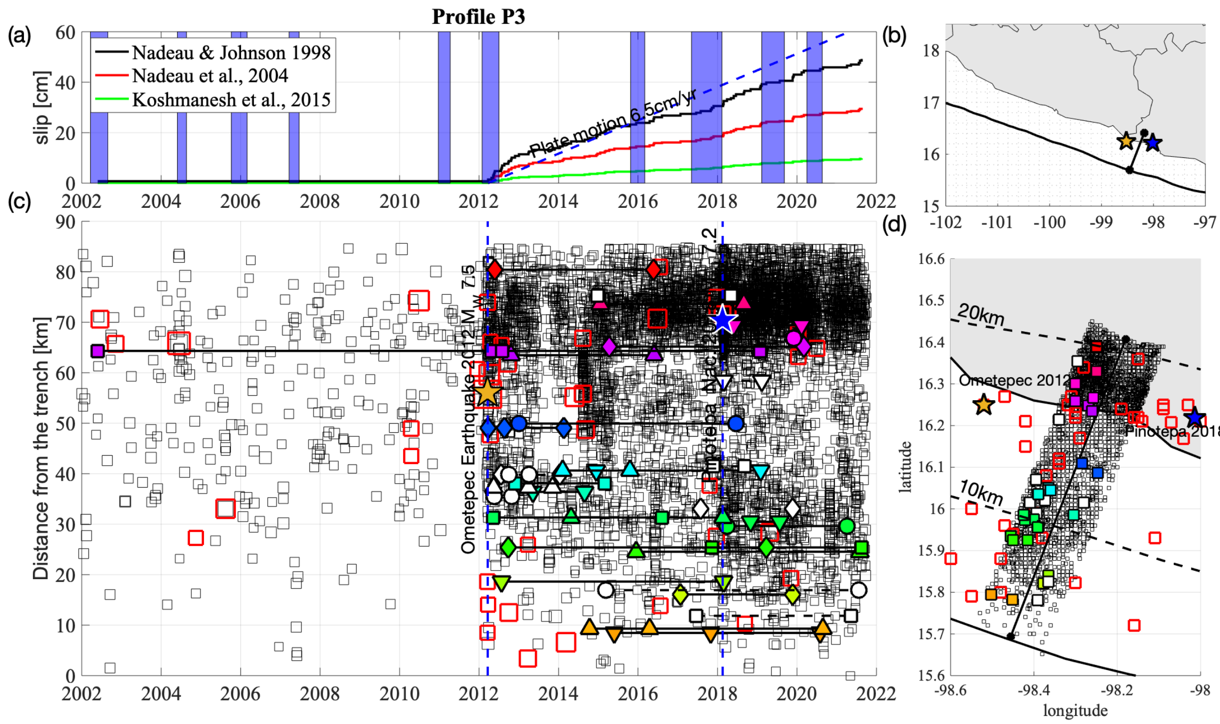

Figure 10. Seismicity and RE activity along profile P3 near the 2018 Pinotepa earthquake (see Fig. 4). (a) Estimated slip rates based on three empirical relationships (see main text), blue shaded areas show the time windows for the SSE in Oaxaca. (b) Location map. (c) Temporal evolution of the seismicity before and after the 2018 Pinotepa earthquake. Black squares indicate the reported seismicity along a 10 km strip at each profile side. Colored symbols indicate the occurrence of RE (white markers show REs below the $M_d < 3.8$). (d) Map view of the profile; the seismicity is shown as empty squares; REs as symbols color-coded by distance from the trench; the stars indicate the location of the 2012 Ometepec (blue) and the 2018 Pinotepa (red) earthquakes; red open squares show seismicity $M \geq 5.0$ within a 30 km distance from the profile.

Figure 13 shows how RE activity evolved in Oaxaca during the interseismic period between the 2012 Ometepec and 2018 Pinotepa earthquakes. Circles indicate the location of the first event detected in each sequence color-coded by decimal date. Blue and thick contours (Figure 13b) indicate the rupture areas of both earthquakes as estimated by aftershocks for the 2012 Ometepec earthquake (UNAM Seismology Group, 2013) and by means of InSAR data and GPS data in the case of the 2018 Pinotepa event (Li et al., 2020), respectively. After the 2012 Ometepec earthquake, new REs appeared near the trench and along the border of the estimated rupture area of the 1968 earthquake (purple contour Fig. 13b), towards the hypocenter of the 2018 Pinotepa earthquake. Furthermore, a significant number of new RE sequences reactivated close to the hypocenter starting in 2017 (blue markers Fig. 13a) and new others appeared at the downdip edge of the second asperity proposed by Li et al. (2020) (yellow box in Fig. 13b).

This intense RE activity strongly suggests the widespread aseismic slip occurring in the plate interface during the years following the 2012 Ometepec earthquake, which certainly reached shallow interface portions (i.e., above 10 km depth and probably next to the trench) and a large part of the 2018 earthquake rupture zone (both onshore and offshore, including the vicinity of the nucleation point) as previously noticed around the hypocentral region in an increase of foreshock seismicity (Cruz-Atienza et al., 2021).

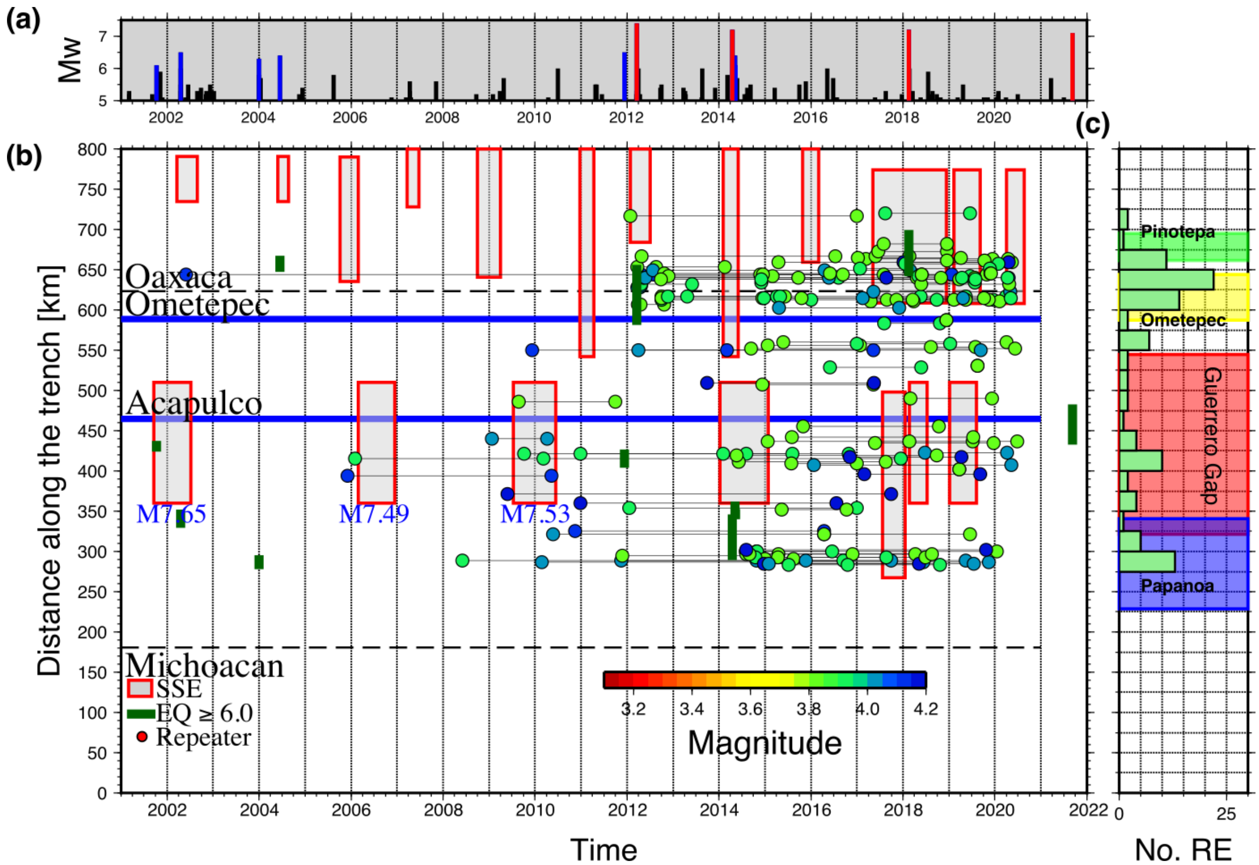

Figure 11. Temporal variations of the repeating earthquakes in Mexico above $M_c \geq 3.8$. (a) Timeline for events with magnitude $5.0 \leq M < 6.0$ (black bars), $6.0 \leq M < 7.0$ (blue bars) and $M \geq 7.0$ (red bars). (b) The *y* axis indicates the distance along the trench as indicated in Figure 4. Shaded areas show the approximate duration and along the trench projected areas. REs are color-coded by magnitude. Green bars indicate earthquake's occurrence and estimated length of earthquakes with a magnitude larger than 6.0. (c) Distribution of REs along the trench.

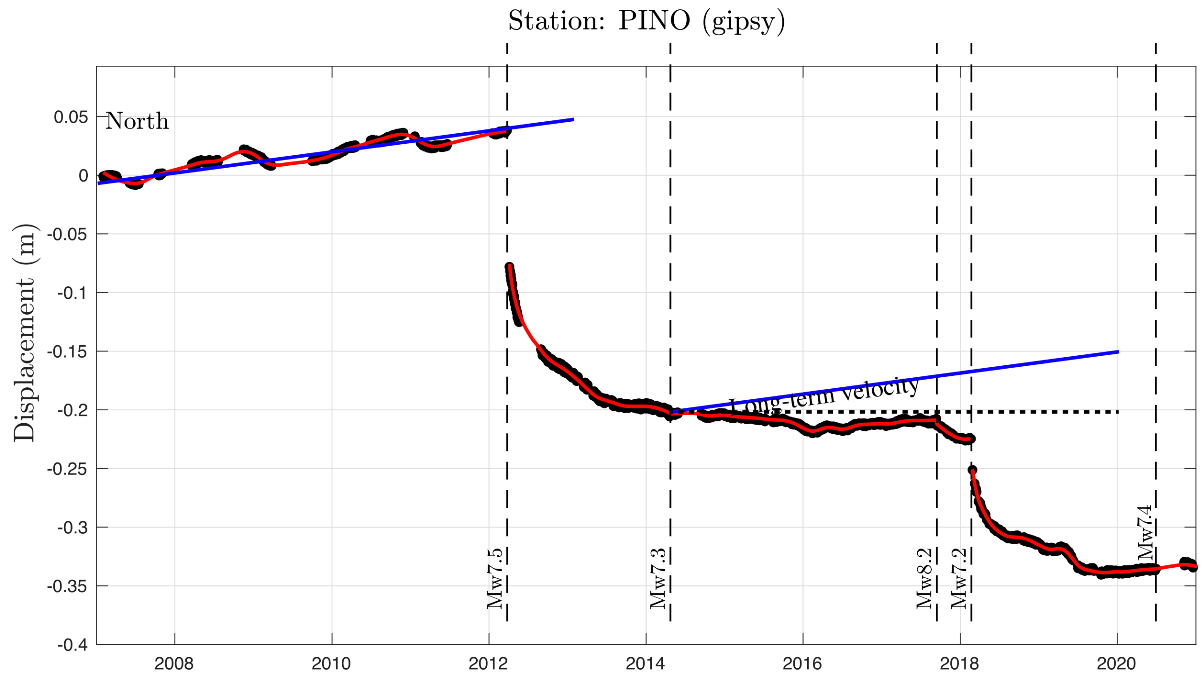

Figure 12. North displacement time series of the closest GPS station (PNIG) to the 2012 Ometepec and 2018 Pinotepa earthquakes. Black dots indicate corrected data, and the red solid line shows the interpolated signal. Dotted vertical lines indicate the time of the major earthquakes during this period (2007-2021). Blue lines show the expected long-term velocity rate before the occurrence of 2012 Ometepec earthquake.

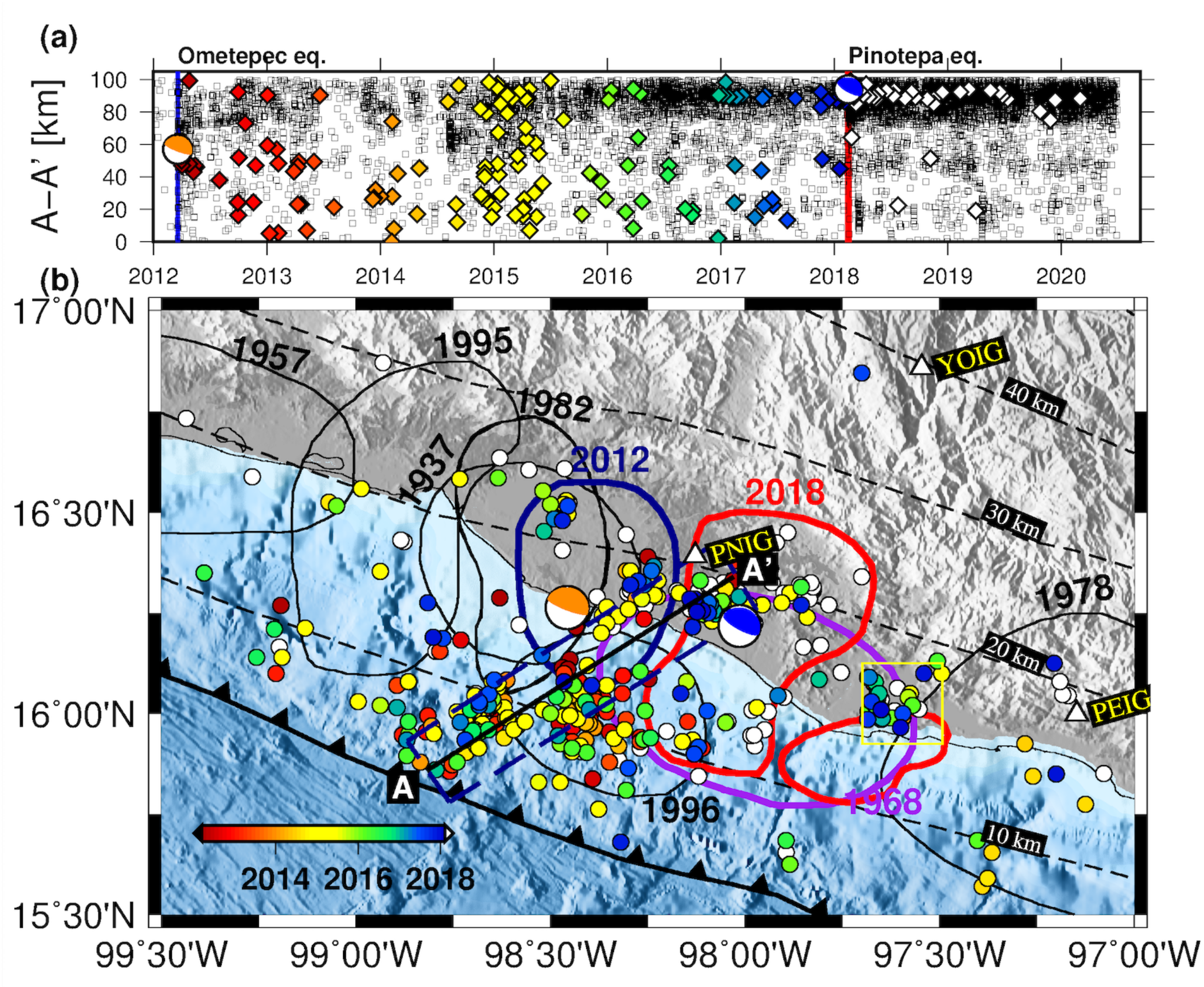

Figure 13. RE activation after the 2012 Ometepec earthquake. (a) Timeline showing the activation of REs along the A-A' profile, empty squares show the background seismicity and colored diamonds indicate the first detected RE location within a sequence color-coded by time. White diamonds indicate those REs that appeared after the 2018 Pinotepa earthquake. (b) Map view. Blue contour and beachball correspond to the rupture area of the 2012 Ometepec earthquake (UNAM Seismology Group, 2013); red contours and beachballs show the rupture area of the 2018 Pinotepa earthquake (Li et al., 2020); purple contour indicates the approximate rupture area of the 1968 earthquake. The yellow box shows a cluster of REs around the second asperity of the 2018 Pinotepa earthquake.

5 Conclusions

Our updated catalog of REs along the Mexican subduction zone provides a valuable tool to investigate how the interplate slip evolved during the last 20 years. This period is particularly interesting given the fact that for about 12 years (2001-2012) the subduction zone did not experience any large thrust earthquakes. During the following nine years (2012-2021), five M7+ class subduction events occurred in Guerrero and Oaxaca regions. We solved for both the stress drop and relative distance of the RE sequences to quantify the size of the asperities, their relative locations, overlap and the associated interplate aseismic slip. Combining coda wave interferometry and solving the resulting distances using a genetic algorithm, we obtained a reliable catalog of REs above the completeness magnitude $M_c \geq 3.8$. From this analysis, the case of the Ometepec-Pinotepa Nacional segment in Oaxaca, where the 2012 earthquake gave rise to a long-lasting, sustained aseismic slip in the region that abruptly increased the RE activity, especially updip (above 15 km depth, mainly offshore), near the trench. During the years following this earthquake, REs activated in a broad region and concentrated next to both the updip edge of the 2018 Pinotepa rupture zone and its hypocenter further downdip. These observations strongly suggest that the shallow, offshore segment of the plate interface continuously slipped after the 2012 earthquake, which may have loaded a large part of the 2018 rupture area. Furthermore, in 2016, several new RE sequences appeared in between the rupture zones of both earthquakes, bordering what may have been the rupture area of the 1968 earthquake. All this activity along with the 2018 Oaxaca SSE that began in June 2017 and swept the downdip portion of the interface (Cruz-Atienza et al., 2021) was certainly responsible for the initiation and rupture propagation of the Pinotepa earthquake. Furthermore, analysis along the GG shows a more dispersed distribution of RE with no significant temporal variations even after the 2014 Papanoa earthquake, whose RE sequences activated mostly sideways (West) of the epicentral area outside the GG. REs in this region are characterized by steady-state behavior with larger recurrence times (1-10 years), likely modulated by the occurrence of SSEs.

Acknowledgments, Samples, and Data

The Servicio Sismológico Nacional (Mexico) earthquake catalog is possible thanks to its personnel and product of the calculations made by its Analysis and Interpretation of Seismic Data department. SSN data was obtained by the Servicio Sismológico Nacional (México); station maintenance, data acquisition, and distribution are thanks to its personnel. GPS data for PINO station was processed by Sara Ivonne Franco at LaGeos laboratory, UNAM. This work was supported by UNAM-PAPIIT IN120220 and IG100921, CONACyT grant 6471, NSF grant EAR-

1735448 and SATREPS-UNAM grant 15543611. We made use of GMT, ZMAP, OBSPy, Tensorflow and SAC software.

References

Audet, P. & Schwartz, S (2013). Hydrologic control of forearc strength and seismicity in the Costa Rican subduction zone. *Nature Geosciences.* 6, 852–855.

Audet, P., & Kim, Y. (2016). Teleseismic constraints on the geological environment of deep episodic slow earthquakes in subduction zone forearcs: A review. *Tectonophysics*, *670*, 1-15.

Anderson, J., Quaas, R., Singh, S. K., Espinosa, J. M., Jiminez, A., Lermo, J., ... & Alcocer, S. (1995). The Copala, Guerrero, Mexico earthquake of September 14, 1995 (M_W= 7.4): a preliminary report. *Seismological Research Letters*, *66*(6), 11-39.

Astiz, L., & Kanamori, H. (1984). An earthquake doublet in Ometepec, Guerrero, Mexico. Physics of the earth and planetary interiors 34.1-2: 24-45.

Barbot, S., Lapusta, N. & Avouac, J.P., 2012. Under the hood of the earthquake machine: Toward predictive modeling of the seismic cycle. *Science*, *336*(6082), pp.707-710.

Brune, J. N. (1970). Tectonic stress and the spectra of seismic shear waves from earthquakes. *Journal of Geophysical Research*, *75*(26), 4997-5009.

Boore, D. M., & Boatwright, J. (1984). Average body-wave radiation coefficients. Bulletin of the Seismological Society of America, 74(5), 1615-1621.

Cattania, C., & Segall, P. (2019). Crack models of repeating earthquakes predict observed moment-recurrence scaling. *Journal of Geophysical Research: Solid Earth*, *124*(1), 476-503.

Chaves, E. J., Schwartz, S. Y., & Abercrombie, R. E. (2020). Repeating earthquakes record fault weakening and healing in areas of megathrust postseismic slip. *Science advances*, *6*(32), eaaz9317.

Chen, K. H., Nadeau, R. M., & Rau, R. J. (2007). Towards a universal rule on the recurrence interval scaling of repeating earthquakes? *Geophysical Research Letters*, *34*(16).

Chen, T., & Lapusta, N. (2009). Scaling of small repeating earthquakes explained by interaction of seismic and aseismic slip in a rate and state fault model. *Journal of Geophysical Research: Solid Earth*, *114*(B1).

Chen, T. & Clayton, R.W., (2012). Structure of central and southern Mexico from velocity and attenuation tomography. *Journal of Geophysical Research: Solid Earth*, *117*(B9).

Corral, A., (2004). Long-term clustering, scaling, and universality in the temporal occurrence of earthquakes. *Physical Review Letters*, *92*(10), p.108501.

Cruz-Atienza, V. M., Husker, A., Legrand, D., Caballero, E., & Kostoglodov, V. (2015). Nonvolcanic tremor locations and mechanisms in Guerrero, Mexico, from energy-based and particle motion polarization analysis. *Journal of Geophysical Research: Solid Earth*, *120*(1), 275-289.

Cruz-Atienza, V. M., Villafuerte, C., & Bhat, H. S. (2018). Rapid tremor migration and pore-pressure waves in subduction zones. *Nature Communications*, *9*(1), 1-13.

Cruz-Atienza, V. M., Tago, J., Villafuerte, C., Wei, M., Garza-Girón, R., Dominguez, L. A., ... & Kazachkina, E. (2021). Short-term interaction between silent and devastating earthquakes in Mexico. *Nature Communications*, *12*(1), 1-14.

Dziewonski, A. M., & Anderson, D. L. (1981). Preliminary reference Earth model. *Physics of the Earth and Planetary Interiors*, *25*(4), 297-356.

Dominguez, L. A., Taira, T. A., & Santoyo, M. A. (2016). Spatiotemporal variations of characteristic repeating earthquake sequences along the Middle America Trench in Mexico. *Journal of Geophysical Research: Solid Earth*, *121*(12), 8855-8870.

Eshelby, J. D. (1957). The determination of the elastic field of an ellipsoidal inclusion, and related problems. *Proceedings of the Royal Society of London. Series A. Mathematical and Physical Sciences*, *241*(1226), 376-396.

Fasola, S.L., Brudzinski, M.R., Holtkamp, S.G., S.E. & Cabral-Cano, E., 2019. Earthquake swarms and slow slip on a sliver fault in the Mexican subduction zone. *Proceedings of the National Academy of Sciences*, *116*(15), pp.7198-7206.

Ferrari, L., Orozco-Esquivel, T., Manea, V., & Manea, M. (2012). The dynamic history of the Trans-Mexican Volcanic Belt and the Mexico subduction zone. *Tectonophysics*, *522*, 122-149.

García, D., Singh, S. K., Herráiz, M., Pacheco, J. F., & Ordaz, M. (2004). Inslab earthquakes of central Mexico: Q, source spectra, and stress drop. Bulletin of the Seismological Society of America, 94(3), 789-802.

García, D., Singh, S. K., Herraiz, M., Ordaz, M., Pacheco, J. F., & Cruz-Jiménez, H. (2009). Influence of subduction zone structure on coastal and inland attenuation in Mexico. *Geophysical Journal International*, *179*(1), 215-230.

Gaite, B., Iglesias, A., Villaseñor, A., Herraiz, M., & Pacheco, J. F., 2012. Crustal structure of Mexico and surrounding regions from seismic ambient noise tomography. *Geophysical Journal International*, *188*(3), pp.1413-1424.

Graham, S.E., DeMets, C., Cabral-Cano, E., Kostoglodov, V., Walpersdorf, A., Cotte, N., Brudzinski, M., McCaffrey, R. & Salazar-Tlaczani, L., 2014. GPS constraints on the M_w= 7.5 Ometepec earthquake sequence, southern Mexico: Coseismic and post-seismic deformation. *Geophysical Journal International*, *199*(1), pp.200-218.

Gualandi, A., Perfettini, H., Radiguet, M., Cotte, N., & Kostoglodov, V. (2017). GPS deformation related to the Mw 7.3, 2014, Papanoa earthquake (Mexico) reveals the aseismic behavior of the Guerrero seismic gap, Geophysical Research Letters, 44, 6039–6047, 2017. https://doi: 10.1002/2017GL072913.

Hughes, L., Chamberlain, C. J., Townend, J., & Thomas, A. M. (2021). A repeating earthquake catalog from 2003 to 2020 for the Raukumara Peninsula, northern Hikurangi subduction margin, New Zealand. Geochemistry, Geophysics, Geosystems, 22, e2021GC009670. https://doi.org/10.1029/2021GC009670

Husker, A., & Davis, P.M., 2009. Tomography and thermal state of the Cocos plate subduction beneath Mexico City. *Journal of Geophysical Research: Solid Earth*, *114*(B4).

Husker, A. L., Kostoglodov, V., Cruz-Atienza, V. M., Legrand, D., Shapiro, N. M., Payero, J. S., ... & Huesca-Pérez, E. (2012). Temporal variations of non-volcanic tremor (NVT) locations in the Mexican subduction zone: Finding the NVT sweet spot. *Geochemistry, Geophysics, Geosystems*, *13*(3).

Husker, A., Ferrari, L., Arango-Galván, C., Corbo-Camargo, F., & Arzate-Flores, J. A. (2018). A geologic recipe for transient slip within the seismogenic zone: Insight from the Guerrero seismic gap, Mexico. *Geology*, *46*(1), 35-38.

Husker, A., Frank, W. B., Gonzalez, G., Avila, L., Kostoglodov, V., & Kazachkina, E. (2019). Characteristic tectonic tremor activity observed over multiple slow slip cycles in the Mexican subduction zone. Journal of Geophysical Research: Solid Earth, 124, 599–608. https://doi-org.pbidi.unam.mx:2443/10.1029/2018JB016517

Iglesias, A., Clayton, R. W., Pérez-Campos, X., Singh, S. K., Pacheco, J. F., Garcia, D., & Valdes-Gonzalez, C. (2010). S wave velocity structure below central Mexico using high-resolution surface wave tomography. Journal of Geophysical Research, 115(B6), 341. http://doi.org/10.1029/2009JB006332

Johnson, P. A., Carpenter, B., Knuth, M., Kaproth, B. M., Le Bas, P.-Y., Daub, E. G., & Marone C. (2012), Nonlinear dynamical triggering of slow slip on simulated earthquake faults with implications to Earth, *Journal of Geophysical Research*, 117, B04310, doi:10.1029/2011JB008594.

Kagan, Y.Y. and Jackson, D.D., 1991. Long-term earthquake clustering. *Geophysical Journal International*, *104*(1), pp.117-133.

Kanamori, H. (1981), *The nature of seismicity patterns before large earthquakes*. In*Earthquake Prediction* (eds. D. W. Simpson and P. G. Richards), Maurice Ewing Series (Amer. Geophys. Union) pp. 1–19.

Kazachkina, E., Kostoglodov, V., Husker, A. & Cotte, N., 2019. Activity of crustal faults and the Xolapa sliver motion in Guerrero–Oaxaca forearc of Mexico, from seismic data. *Earth, Planets and Space*, *71*(1), p.104.

Kazachkina, E., Kostoglodov, V., Cotte, N., Walpersdorf, A., Ramirez-Herrera, M.T., Gaidzik, K., Husker, A.L. & Santiago, J.A., 2020. Active 650-km long fault system and Xolapa sliver in Southern Mexico. *Frontiers in Earth Science*, *8*, p.155.

Keilis-Borok, V.I., Knopoff, L. and Rotvain, I.M., 1980. Bursts of aftershocks, long-term precursors of strong earthquakes. *Nature*, *283*(5744), pp.259-263.

Kim, Y., Clayton, R. W., Asimow, P. D., & Jackson, J. M. (2013). Generation of talc in the mantle wedge and its role in subduction dynamics in central Mexico. Earth and Planetary Science Letters, 384, 81–87. http://doi.org/10.1016/j.epsl.2013.10.006

Khoshmanesh, M., Shirzaei, M., & Nadeau, R. M. (2015). Time-dependent model of aseismic slip on the central San Andreas Fault from InSAR time series and repeating earthquakes. *Journal of Geophysical Research: Solid Earth*, *120*(9), 6658-6679.

Konca, A. O., Avouac, J. P., Sladen, A., Meltzner, A. J., Sieh, K., Fang, P., ... & Helmberger, D. V. (2008). Partial rupture of a locked patch of the Sumatra megathrust during the 2007 earthquake sequence. *Nature*, *456*(7222), 631-635.

Kostoglodov V. & Pacheco J. (1999). Cien Años de Sismicidad en México, Instituto de Geofísica, UNAM, México City.

Kostoglodov, V., Husker, A., Shapiro, N. M., Payero, J. S., Campillo, M., Cotte, N., & Clayton, R. (2010). The 2006 slow slip event and nonvolcanic tremor in the Mexican subduction zone. *Geophysical Research Letters*, *37*(24).

Legrand, D., Iglesias, A., Singh, S. K., Cruz-Atienza, V., Yoon, C., Dominguez, L. A., ... & Castro-Artola, O. (2021). The influence of fluids in the unusually high-rate seismicity in the Ometepec segment of the Mexican subduction zone. *Geophysical Journal International*, *226*(1), 524-535.

Li, Y., Shan, X., Zhu, C., Qiao, X., Zhao, L., & Qu, C. (2020). Geodetic Model of the 2018 M_w 7.2 Pinotepa, Mexico, Earthquake Inferred from InSAR and GPS Data. *Bulletin of the Seismological Society of America 110(3), 1115-1124*. http://doi.org/10.1785/0120190101

Lonsdale, P. (2005). Creation of the Cocos and Nazca plates by fission of the Farallon plate. *Tectonophysics*, *404*(3-4), 237-264. https://doi.org/10.1016/j.tecto.2005.05.011

Ordaz, M., & Singh, S. K. (1992). Source spectra and spectral attenuation of seismic waves from Mexican earthquakes, and evidence of amplification in the hill zone of Mexico City. *Bulletin of the Seismological Society of America*, *82*(1), 24-43.

Ortiz, M., Singh, S. K., Kostoglodov, V., & Pacheco, J. (2000). Source areas of the Acapulco-San Marcos, Mexico earthquakes of 1962 (M 7.1; 7.0) and 1957 (M 7.7), as constrained by tsunami and uplift records. *Geofísica Internacional*, *39*(4), 337-348.

Pardo, M. & Suárez, G., 1995. Shape of the subducted Rivera and Cocos plates in southern Mexico: Seismic and tectonic implications. *Journal of Geophysical Research: Solid Earth*, *100*(B7), pp.12357-12373.

Payero, J. S., Kostoglodov, V., Shapiro, N., Mikumo, T., Iglesias, A., Pérez-Campos, X., & Clayton, R. W. (2008). Nonvolcanic tremor observed in the Mexican subduction zone. *Geophysical Research Letters*, *35*(7).

Pérez-Campos, X., Kim, Y., Husker, A., Davis, P. M., Clayton, R. W., Iglesias, A., Pacheco, J. F., Singh, S. K., Manea, V. C., & Gurnis M. (2008), Horizontal subduction and truncation of the Cocos Plate beneath central Mexico, *Geophysical Research Letters*, 35, L18303, doi:10.1029/2008GL035127.

Pérez-Campos, X., Espíndola, V. H., Pérez, J., Estrada, J. A., Monroy, C. C., & Bello, D. (2018). The Mexican national seismological service: An overview. *Seismological Ressearch Letters*, *89*, 318–323.

Plata-Martínez, R., Pérez-Campos, X., & Singh, S. K. (2019). Spatial distribution of radiated seismic energy of three aftershocks sequences at Guerrero, Mexico, subduction zone. *Bulletin of the Seismological Society of America*, *109*(6), 2556-2566.

Plata-Martínez, R., Ide, S., Shinohara, M., Garcia, E. S., Mizuno, N., Dominguez, L. A., ... & Ito, Y. (2021). Shallow slow earthquakes to decipher future catastrophic earthquakes in the Guerrero seismic gap. *Nature communications*, *12*(1), 1-8.

Poupinet, G., Ellsworth, W. L., & Frechet, J. (1984). Monitoring velocity variations in the crust using earthquake doublets: An application to the Calaveras Fault, California. *Journal of Geophysical Research: Solid Earth*, *89*(B7), 5719-5731.

Prieto, G. A., R. L. Parker, F. L. Vernon. (2009), A Fortran 90 library for multitaper spectrum analysis, Computers and Geosciences, 35, pp. 1701-1710. doi:10.1016/j.cageo.2008.06.007.

Segou, M., & Parsons, T. (2018). Testing earthquake links in Mexico from 1978 to the 2017 M= 8.1 Chiapas and M= 7.1 Puebla shocks. *Geophysical Research Letters*, *45*(2), 708-714.

Radiguet, M., Cotton, F., Vergnolle, M., Campillo, M., Walpersdorf, A., Cotte, N., & Kostoglodov, V., (2012). Slow slip events and strain accumulation in the Guerrero gap, Mexico. *Journal of Geophysical Research: Solid Earth*, *117*(B4).

Radiguet, M., Perfettini, H., Cotte, N., Gualandi, A., Valette, B., Kostoglodov, V., Lhomme, T., Walpersdorf, A., Cano, E.C. & Campillo, M., (2016). Triggering of the 2014 M w 7.3 Papanoa earthquake by a slow slip event in Guerrero, Mexico. *Nature Geoscience*, *9*(11), pp.829-833.

Ramírez-Herrera, M.T., Gaidzik, K., Forman, S., Kostoglodov, V., Bürgmann, R., Johnson, C. W.; Relating the long-term and short-term vertical deformation across a transect of the forearc in the central Mexican subduction zone (2018). *Geosphere*; 14 (2): 419–439. https://doi.org/10.1130/GES01446.1

Rivet, D., Campillo, M., Radiguet, M., Zigone, D., Cruz-Atienza, V., Shapiro, N. M., ... & Daub, E. (2014). Seismic velocity changes, strain rate and non-volcanic tremors during the 2009–2010 slow slip event in Guerrero, Mexico. *Geophysical Journal International*, *196*(1), 447-460.

Santoyo, M. A., Singh, S. K., Mikumo, T., & Ordaz, M. (2005). Space–time clustering of large thrust earthquakes along the Mexican subduction zone: an evidence of source stress interaction. *Bulletin of the seismological society of America*, *95*(5), 1856-1864.

Sawires, R., Santoyo, M. A., Peláez, J. A., & Fernández, R. D. C. (2019). An updated and unified earthquake catalog from 1787 to 2018 for seismic hazard assessment studies in Mexico. *Scientific data*, *6*(1), 1-14.

Shearer, P. M. (2019). *Introduction to seismology*. Cambridge university press.

Singh, S. K., Astiz, L., & Havskov, J. (1981). Seismic gaps and recurrence periods of large earthquakes along the Mexican subduction zone: A reexamination. *Bulletin of the Seismological Society of America*, *71*(3), 827-843.

Singh, S. K., Pacheco, J., Courboulex, F., & Novelo, D. A. (1997). Source parameters of the Pinotepa Nacional, Mexico, earthquake of 27 March, 1996 (Mw= 5.4) estimated from near-field recordings of a single station. *Journal of Seismology*, *1*(1), 39-45.

Singh, S. K., Reinoso, E., Arroyo, D., Ordaz, M., Cruz-Atienza, V., Pérez-Campos, X., ... & Hjörleifsdóttir, V. (2018). Deadly intraslab Mexico earthquake of 19 September 2017 (M w 7.1): Ground motion and damage pattern in Mexico City. *Seismological Research Letters*, *89*(6), 2193-2203.

Skinner, S. M., & Clayton, R. W. (2011). An Evaluation of Proposed Mechanisms of Slab Flattening in Central Mexico. Pure and Applied Geophysics, 168(8-9), 1461–1474. http://doi.org/10.1007/s00024-010-0200-3

Stein, S. & Liu, M., (2009). Long aftershock sequences within continents and implications for earthquake hazard assessment. *Nature*, *462*(7269), p.87.

Storn, R., & Price, K. (1997). Differential evolution–a simple and efficient heuristic for global optimization over continuous spaces. *Journal of global optimization*, *11*(4), 341-359.

Stubailo, I., Beghein, C., & Davis, P. M. (2012). Structure and anisotropy of the Mexico subduction zone based on Rayleigh-wave analysis and implications for the geometry of the Trans-Mexican Volcanic Belt. *Journal of Geophysical Research: Solid Earth*, *117*(B5).

Snieder, R., & Vrijlandt, M. (2005). Constraining the source separation with coda wave interferometry: Theory and application to earthquake doublets in the Hayward fault, California. Journal of Geophysical Research-Solid Earth, 110(B4). https://doi.org/10.1029/2004JB003317

Servicio Sismológico Nacional (SSN). (2021). Catálogo de sismos. Retrieved from http://www2.ssn.unam.mx:8080/catalogo/. https:/doi.org/10.21766/SSNMX/EC/MX

Storn, R. & Price, K. (1997). "Differential evolution - a simple and efficient heuristic for global optimization over continuous spaces". Journal of Global Optimization. 11 (4): 341–359. https://doi.org/10.1023/A:1008202821328.

Spica, Z., Perton, M., Calò, M., Legrand, D., Córdoba-Montiel, F. & Iglesias, A. (2016). 3-D shear wave velocity model of Mexico and south US: bridging seismic networks with ambient noise cross-correlations (C1) and correlation of coda of correlations (C3). *Geophysical Journal International*, *206*(3), pp.1795-1813.

Sawires, R., Santoyo, M. A., Peláez, J. A., & Corona Fernández, R. D. (2019). An updated and unified earthquake catalog from 1787 to 2018 for seismic hazard assessment studies in Mexico. *Scientific data*, *6*(1), 1-14.

Suárez, G., Santoyo, M. A., Hjorleifsdottir, V., Iglesias, A., Villafuerte, C., & Cruz-Atienza, V. M. (2019). Large scale lithospheric detachment of the downgoing Cocos plate: The 8 September 2017 earthquake (Mw 8.2). Earth and Planetary Science Letters, 509, 9-14.

Tepp, G. (2018). A repeating event sequence alarm for monitoring volcanoes. *Seismological Research Letters*, *89*(5), pp.1863-1876.

Madariaga, Raul (1976). Dynamics of an expanding circular fault. *Bulletin of the Seismological Society of America,* 66, 3, 639-666.

Materna, K., Taira, T., & Bürgmann, R. (2018). Aseismic transform fault slip at the Mendocino Triple Junction from characteristically repeating earthquakes. Geophysical Research Letters, 45. https://doi.org/10.1002/2017GL075899.

Mavrommatis, A. P., Segall, P., Uchida, N., & Johnson, K. M. (2015), Long-term acceleration of aseismic slip preceding the M_w 9 Tohoku-oki earthquake: Constraints from repeating earthquakes, *Geophysical. Research Letters*, 42, 9717– 9725, doi:10.1002/2015GL066069.

Melgar, D., & Pérez-Campos, X. (2011). Imaging the Moho and subducted oceanic crust at the Isthmus of Tehuantepec, Mexico, from receiver functions. *Pure and applied geophysics*, *168*(8), 1449-1460.

Melgar, D., Ruiz-Angulo, A., Garcia, E.S., Manea, M., Manea, V.C., Xu, X., Ramirez-Herrera, M.T., Zavala-Hidalgo, J., Geng, J., Corona, N. & Pérez-Campos, X., (2018a). Deep embrittlement and complete rupture of the lithosphere during the M w 8.2 Tehuantepec earthquake. *Nature Geoscience*, *11*(12), pp.955-960.

Melgar, D., Pérez-Campos, X., Ramirez-Guzman, L., Spica, Z., Espíndola, V. H., Hammond, W. C., & Cabral-Cano, E. (2018b). Bend faulting at the edge of a flat slab: The 2017 Mw7. 1 Puebla-Morelos, Mexico earthquake. *Geophysical Research Letters*, *45*(6), 2633-2641.

Meng, L., Huang, H., Xie, Y., Bao, H., & Dominguez, L. A. (2019). Nucleation and kinematic rupture of the 2017 Mw 8.2 Tehuantepec earthquake. *Geophysical Research Letters*, *46*(7), 3745-3754.

Moreno, M., Haberland, C., Oncken, O., Rietbrock, A., Angiboust, S., & Heidbach, O. (2014). Locking of the Chile subduction zone controlled by fluid pressure before the 2010 earthquake. *Nature Geoscience*, *7*(4), 292-296.

Nadeau, R. M., & Johnson, L. R. (1998). Seismological studies at Parkfield VI: Moment release rates and estimates of source parameters for small repeating earthquakes. *Bulletin of the Seismological Society of America*, *88*(3), 790-814.

Nadeau, R. M., & McEvilly, T. V. (1999). Fault slip rates at depth from recurrence intervals of repeating microearthquakes. *Science*, *285*(5428), 718-721.

Nadeau, R. M., & McEvilly, T. V. (2004). Periodic pulsing of characteristic microearthquakes on the San Andreas fault. *Science*, *303*(5655), 220-222.

Nishenko, S. P., & Singh, S. K. (1987). The Acapulco-Ometepec, Mexico, earthquakes of 1907-1982: Evidence for a variable recurrence history. *Bulletin of the Seismological Society of America*, *77*(4), 1359-1367.

Universidad Nacional Autónoma de México (UNAM) Seismology Group (2013). Ometepec-Pinotepa Nacional, Mexico earthquake of 20 March 2012 (Mw 7.5): A preliminary report, *Geofísica Internacional* 52, 172–196.

Universidad Nacional Autónoma de México (UNAM) Seismology Group (2015). Papanoa, Mexico earthquake of 18 April 2014 (M_W 7.3). *Geofísica Internacional,* 363-386.

Uchida, N., Shimamura, K., Matsuzawa, T., & Okada, T. (2015). Postseismic response of repeating earthquakes around the 2011 Tohoku-oki earthquake: Moment increases due to the fast loading rate. *Journal of Geophysical Research: Solid Earth*, *120*, 259–274. https://doi.org/10.1002/2013JB010933.

Uchida, N., Kalafat, D., Pinar, A., & Yamamoto, Y. (2019). Repeating earthquakes and interplate coupling along the western part of the North Anatolian Fault. *Tectonophysics*, *769*, 228185.

Uchida, N. (2019). Detection of repeating earthquakes and their application in characterizing slow fault slip. *Progress in Earth and Planetary Science*, *6*(1), 1-21.

Vergnolle, M., Walpersdorf, A., Kostoglodov, V., Tregoning, P., Santiago, J.A., Cotte, N. & Franco, S.I. (2010). Slow slip events in Mexico revised from the processing of 11 year GPS observations. *Journal of Geophysical Research: Solid Earth*, *115*(B8).

Vidale, J. E., Ellsworth, W. L., Cole, A., & Marone, C. (1994). Variations in the rupture process with recurrence interval in a repeated small earthquake. *Nature*, *368*(6472), 624-626.

Villafuerte, C., & Cruz-Atienza, V. M. (2017). Insights into the causal relationship between slow slip and tectonic tremor in Guerrero, Mexico. *Journal of Geophysical Research: Solid Earth*, *122*, 6642–6656. https://doi.org/10.1002/2017JB014037.

Wang, K., & Dixon, T. (2004). "Coupling" semantics and science in earthquake research, *Eos Trans. AGU*, 85(18), 180– 180, https://doi.org/10.1029/2004EO180005.

Wang, Q., Jackson, D.D. and Zhuang, J., 2010. Missing links in earthquake clustering models. *Geophysical Research Letters*, *37*(21).

Warren-Smith, E., Fry, B., Wallace, L., Chon, E., Henrys, S., Sheehan, A., ... & Lebedev, S. (2019). Episodic stress and fluid pressure cycling in subducting oceanic crust during slow slip. *Nature Geoscience*, *12*(6), 475-481.

Wyss, M. and Habermann, R.E., 1988. Precursory seismic quiescence. *Pure and Applied Geophysics*, *126*(2-4), 319-332.